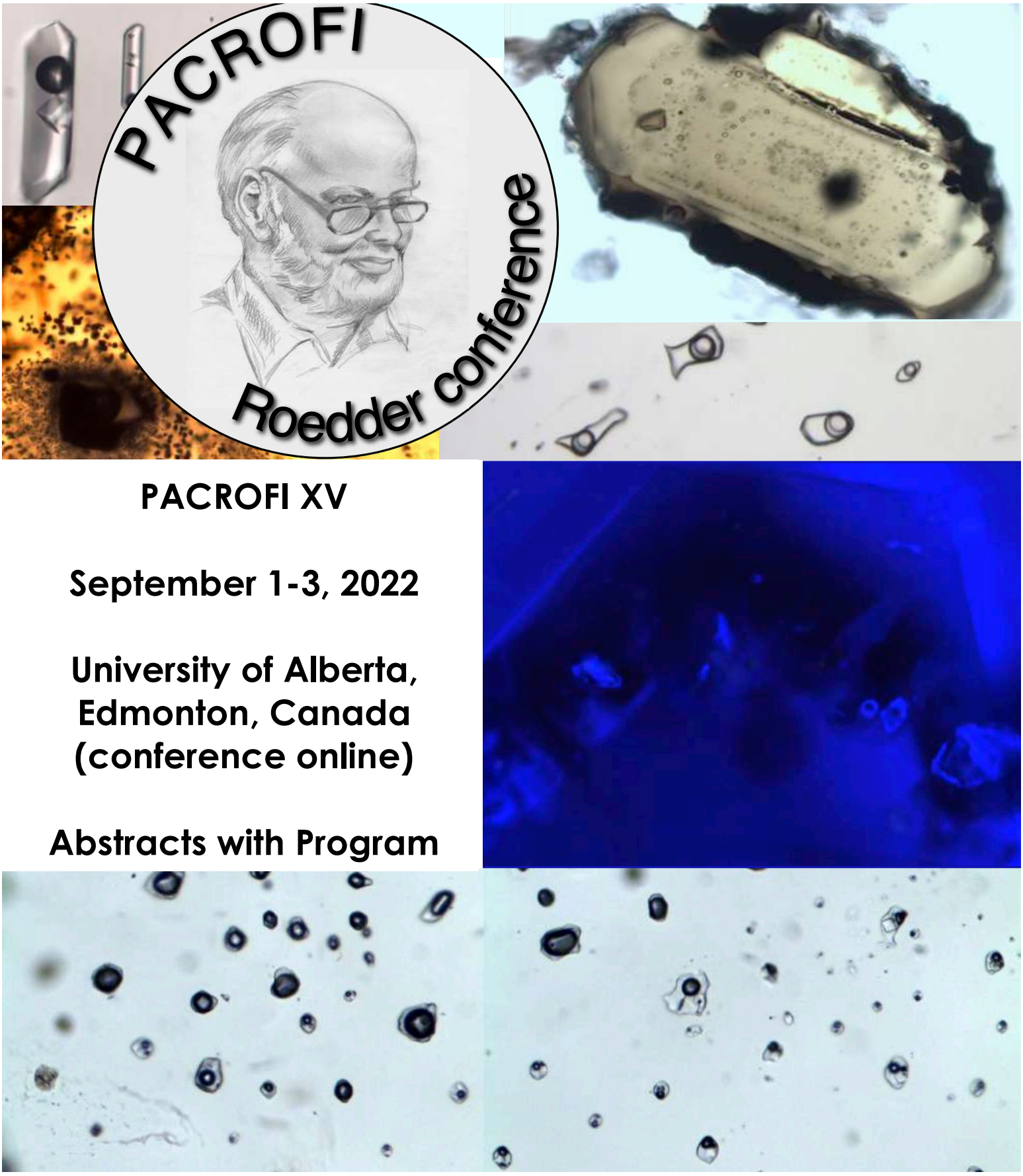

PACROFI XV

September 1-3, 2022

University of Alberta, Edmonton, Canada (conference online)

Abstracts with Program

Pan-American Current Research on Fluid and Melt Inclusions

PACROFI XV

The XVth Edwin Roedder **P**an-**A**merican
Current **R**esearch on **F**luid (and melt) **I**nclusions
Conference

September 1-3, 2022
Edmonton, Canada (online)

Conveners: Pilar Lecumberri-Sanchez and
Matthew Steele-MacInnis

University of Alberta, Edmonton, Canada

Abstracts with Program

Edited by Matthew Steele-MacInnis,

Pilar Lecumberri-Sanchez, and Marko Szmihelsky

Local Organizing Committee (University of Alberta)

Pilar Lecumberri-Sanchez
Matthew Steele-MacInnis
Marko Szmihelsky
Spencer Poulette

PACROFI XV Advisory Board

Bob Bodnar – Virginia Tech
Dan Marshall – Simon Fraser University
Andras Fall – UT Austin
Dan Kontak – Laurentian University
Jake Hanley – St Mary's Universtiy
Martin Appold – University of Missouri
Iain Samson – University of Windsor

ACKNOWLEDGMENTS

The XVth Edwin Roedder PACROFI conference was originally scheduled to take place at the University of Calgary in 2020, but was of course derailed by the onset of the global COVID-19 pandemic. That earlier iteration of the conference was co-organized by **Ben Tutolo** (University of Calgary) and **Dan Marshall** (Simon Fraser University), in addition to Pilar Lecumberri-Sanchez and Matt Steele-MacInnis – therefore, Ben and Dan are owed huge thanks for their efforts. In addition, the Calgary conference would have been financially supported by **Horiba Scientific**, and their support is also gratefully acknowledged.

Alongside the earlier Calgary conference, a plan was in place for a two-day short course on applications of fluid and melt inclusions in geologic studies, and this course was supported by the **Geological Association of Canada**, the **Mineral Deposits Division**, the **Mineralogical Association of Canada** and **Horiba Scientific**. We gratefully acknowledge each of these organizations for their support. The course was co-organized by **Dan Kontak**, in addition to Pilar and Matt. The course did eventually take place, in online format, during the 2021 GAC-MAC conference in London, Ontario (Canada); and an associated book was published by the **Mineralogical Association of Canada** under the Topics in Mineral Sciences series (volume 49 – ISBN 978-0-921294-63-4). We gratefully thank **MAC**, as well as series editor **Rob Raeside** and business manager **Johanne Caron**, for making this course and volume possible.

Finally, many thanks to our advisory board—**Bob Bodnar, Dan Marshall, Andras Fall, Dan Kontak, Jake Hanley, Iain Samson and Martin Appold**—for their many contributions to making this conference possible, especially in light of the many ups and downs that have come with the COVID-19 pandemic and its effects on international travel and conferences. Special thanks to **Bob Bodnar** for also graciously agreeing to lead the pre-conference short course.

We are delighted that PACROFI XV is (finally!) taking place.

Contents

Program

Note: All times refer to MDT time zone (GMT-6)

Thursday, September 1st, 2022

Short Course: Introduction to Fluid and Melt Inclusions

Principal Instructor: Bob Bodnar (Virginia Tech)

7:00	*Introduction to fluid inclusions, including FI types, FIAs, and basic microthermometric techniques (Bodnar)*
08:45	*Phase equilibria of common fluid systems: H_2O; H_2O-NaCl; CO_2; H_2O-CO_2; H_2O-NaCl-CO_2 (Bodnar)*
11:00	*Programs and spreadsheets available to interpret FI microthermometric data (Steele-MacInnis)*
12:45	*Analytical techniques for FI, with emphasis on Raman and LAICPMS (Bodnar)*
1:45	*Introduction to melt inclusions and applications (Bodnar)*
2:45	*Questions and discussion*

End of short course

Friday, September 2nd, 2022

07:50 **Opening remarks**

SESSION 1: Chaired by Katie McFall (University College London)

08:00 ***Fluid inclusion study of Ag and Sn bearing hydrothermal veins along the shear zone of Main Central Thrust in Himachal Himalaya, India***
Shruti Rana, Rajesh Sharma

08:20 ***Ore forming fluid characteristics of orogenic gold deposits from Saqqez–Sardasht–Piranshahr gold field, north-west of Iran***
Shojaeddin Niroomand, Hossein Ali Tajeddin, Majid Soleymani, Dunya Maronsi

08:40 ***The Timing and Setting of Copper mineralization in the Timna Igneous Complex, Northernmost Arabian-Nubian Shield***
Alon Elhadad, Yevgeny Vapnik, Bar Elisha, Itai Haviv, Yaron Katzir

09:00 ***Fluid chemistry of the Archean Chibougamau porphyry-type Cu(-Au) system: An aqueous-carbonic magmatic hydrothermal ore system***
Daniel Kontak, Lucy Mathieu, Alexandre Crépon

09:20 **Break**

SESSION 2: Chaired by Eszter Sendula (Arctic University of Norway)

09:40 ***Halite fluid inclusions: a gateway to atmospheric oxygen levels and shallow marine environments in deep time***
Nigel Blamey, Uwe Brand, Amy Lefebvre, Audrey Morrison

10:00 ***The End Ordovician Icehouse and the First Mass Extinction of the Phanerozoic: Its History Recorded in Halite***
Audrey Morrison, Amy Lefebvre, Ariel Patter, Alyssa Davis Uwe Brand, Nigel Blamey, Jisuo Jin

10:20 ***Raman Spectroscopic Properties of Aqueous Chloride Solutions: Chlorides of Alkali, Alkaline Earth, and First Row Transition Metals***
Spencer Poulette, Matthew Steele-MacInnis

10:40 ***A fluid inclusion outlook on the petroleum migration of the Cretaceous Potiguar Basin, Brazilian Equatorial Margin***
André Luiz Silva Pestilho, Lena Virgínia Soares Monteiro

11:00 ***Break***

12:00 **Virtual poster session**

Temporal Evolution of Fluid on a High-sulfidation Hydrothermal System Related to Alkalic Magmatism-Silver Pond Lawyers Property, Toodoggone District, North-Central British Columbia
Sinan Canbulat, Matthew Steele-MacInnis, Pilar Lecumberri-Sanchez, Pascal Voegeli

Fluid Inclusion Analysis of Halite from the Early Cambrian Amadeus Basin of Australia
Amy Lefebvre, A. Morrison, N.J.F. Blamey, U. Brand

SESSION 3: Chaired by Mitchell Bennett (US Geological Survey)

12:30 ***Determining Pressure and Temperature of Gold-Related Fluid inclusion Formation at Salmita Mine, NWT***
Spencer Poulette, Matthew Steele-MacInnis

12:50 ***Muscovite crystals in carbonic fluid inclusions, Red Lake mine trend, Ontario, Canada***
Marko Szmihelsky, Matthew Steele-MacInnis, Guoxiang Chi, Spencer Poulette

13:10 ***Fluid inclusion study along the Midwest Trend, Athabasca Basin, Saskatchewan***
Daniel Ferguson, Guoxiang Chi, Charles Normand, Yumeng Wang, Remy Chemillac, John Robbins, Patrick Ledru

13:30 ***Factors controlling the formation of unconformity-related uranium deposits in the Proterozoic Athabasca Basin – insights from fluid inclusion studies***
Guoxiang Chi, Haixia Chu, Morteza Rabiei, Eric Potter, Duane Petts, Daniel Ferguso

End of day 1

Saturday, September 3rd, 2022

SESSION 4: Chaired by Andras Fall (UT Austin)

08:00 ***Characteristics of fluid inclusions and Pressure evolution in the second member of Dengying in Pengtan area, Sichuan Basin, China***
Junjia Fan, Xuesong Lu, Jacques Pironon, Alexy Elias Bahnan, Xiuyan Liu, Xinzhi Ma, Lili Gui

08:20 ***Fluid Inclusion Technique For Basin Modeling—A Case Study***
V. Nandakumar, Shivapriya S., Silpa Thankan

08:40 ***Fluid inclusions trapping temperatures as calibration tools in modeling sedimentary basins***
Alexy Elias Bahnan, Metzger Mombo Mouketo, Salim Allouti, Raymond Michels, Jacques Pironon

09:00 ***Fluid modeling and U-Pb dating constraints on fluid evolution history in 1D basin modeling framework***
Xiuyan Liu, Jacques Pironon, Alexy Elias Bahnan

09:20 ***Break***

SESSION 5: Chaired by Penny Wieser (UC Berkeley)

09:40 ***Evidence for infiltrative contact metasomatism between silicate melts and carbonates at Chating, China***

Xinyue Xu, Matthew Steele-MacInnis, Xiaochun Xu, Marko Szmihelsky

10:00 ***Melt inclusions in Catalina 008: Studying carbonaceous chondrite from Atacama Desert with Raman Spectroscopy***
Claudia Aravena-González, Daniel Moncada, Rodrigo Martínez

10:20 ***High-temperature inclusions in IOA and IOCG-type deposits***
Xinyue Xu, Matthew Steele-MacInnis, Wyatt Bain, Marko Szmihelsky

10:40 ***A melt inclusion study of rhyolitic volcanics in the Bousquet Formation, Doyon-Bousquet-LaRonde mining camp, Abitibi Subprovince, Québec: Insight into Archean magmatic processes***
Jacob Hanley, Daniel Meagher, Kevin Neyedley, Zoltán Zajacz Alexandra Tsay, and Patrick Mercier-Langevin

11:00 ***Break***

12:00 ***Plenary session***

SESSION 6: Chaired by Stephanie Forstner (UT Austin)

12:30 ***Pilot study in the use of synchrotron nano-CT to identify accidental mineral inclusions in fluorite-hosted fluid inclusions from the Illinois-Kentucky Mississippi Valley-type ore district***
Martin Appold, Wesley Clarkston, Sarah Smith-Schmitz, Hector Lamadrid

12:50 ***Evidence of deep-sourced volatiles in the diagenetic evolution of the Aptian carbonates of Santos Basin, Brazil***
André Pluiz Silva Pestilho, Dorval Dias Filho, Volker Lüders, Isabela de O Carmo, Anna Eliza Dias, Leonardo Tedeshi, Bruno de Carvalho, Erica de Moraes, Delano Ibanez, Gustavo Garcia

13:10 ***The healing power of Faden quartz (Zhob District, Pakistan)***
Andras Fall, Estibalitz Ukar

End of conference

Abstracts

Pilot study in the use of synchrotron nano-CT to identify accidental mineral inclusions in fluorite-hosted fluid inclusions from the Illinois-Kentucky Mississippi Valley-type ore district

Martin S. APPOLD[1], Wesley C. CLARKSTON[1], Sarah E. SMITH-SCHMITZ[2], Hector M. LAMADRID[1]

[1]*Department of Geological Sciences, University of Missouri, Columbia, Missouri, USA*

[2]*Bureau of Geology & Mineral Resources, New Mexico Institute of Mining & Technology, Socorro, New Mexico, USA*

E-mail: appoldm@missouri.edu

Knowledge of the metal content of ore fluids is vital to answering a variety of fundamental genetic questions about ore deposits and is commonly pursued by analyzing fluid inclusions using LA-ICP-MS. However, the calculated metal concentrations from LA-ICP-MS analyses are commonly inconsistent within fluid inclusion assemblages (FIA's), despite the concentrations of other elements, bulk salinity, and homogenization temperature being consistent, and peaks in the LA-ICP-MS metal responses coinciding closely with the Na response, a known fluid inclusion aqueous solute (see Appold, 2021 and references therein). Further, in the Illinois-Kentucky Mississippi Valley-type (MVT) district, the proportion of Cu relative to Zn and Pb in many fluid inclusions is inconsistent with these elements' relative aqueous solubilities and proportions in the ore deposits. These observations suggest that metals in many fluid inclusions analyzed in LA-ICP-MS studies may not actually exist as dissolved species in aqueous solution but rather as accidental mineral inclusions ("accidentals"), i.e. fragments of earlier formed metal-rich minerals that became entrained within the ore fluids and ultimately within fluid inclusions (Roedder, 1984). Alternatively, the inconsistent metal concentrations within FIA's may reflect low precision of LA-ICP-MS in measuring trace element concentrations in fluid inclusions. However, if accidentals were truly responsible for the high fluid inclusion metal concentrations reported in some LA-ICP-MS studies, then the inferred ore fluids would not have been as rich in dissolved metals as previously thought, implying that the ore fluids may not have been as unusual compared to other crustal fluids as previously thought, that more time to form the ore deposits would have been needed, and that ore formation by mechanisms that require simultaneous transport of metals and reduced sulfur are more likely.

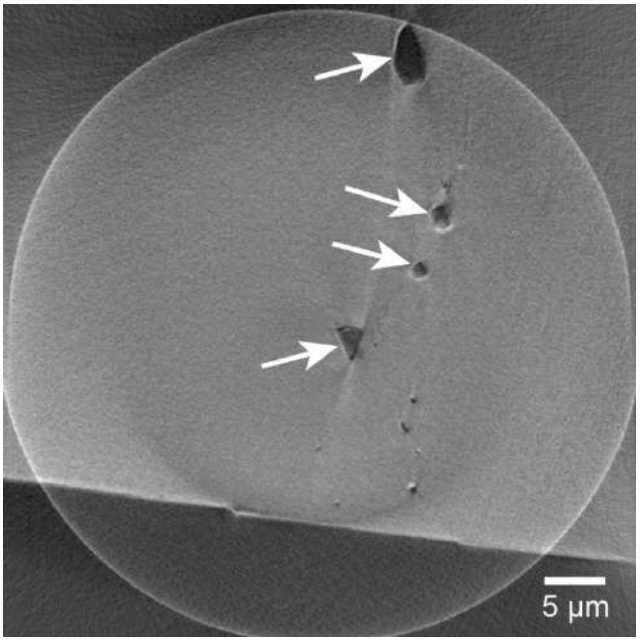

Figure 1. Synchrotron X-ray nano-CT image of fluorite from the Illinois-Kentucky district. White arrows point to the largest fluid inclusions in the image.

Synchrotron X-ray nano-computed-tomography (nano-CT) is a potential tool for determining whether accidental mineral inclusions larger than about 40 nm (the current resolution of the technique) exist in fluid inclusions. Fluid inclusions in sphalerite have previously been imaged near this resolution by Yao et al. (2015), though not for the purpose of detecting accidentals. A pilot study has been conducted by the present authors to test the feasibility of synchrotron nano-CT for imaging fluid inclusions by analyzing fluorite from the Illinois-Kentucky district. In this study, several grains of fluorite averaging about 100 µm in diameter were

mounted on the tips of hypodermic needles using epoxy. Nano-CT imaging was performed at the Advanced Photon Source at Argonne National Laboratory, USA using Beamline 32-ID-B,C. Each nano-CT analysis of a mineral grain produced thousands of two-dimensional image slices in TIFF format, which were processed using the Object Research Systems Dragonfly software. An example of an image slice is shown in Figure 1, which contains several fluid inclusions, the largest of which are pointed out by white arrows. In the rendering shown in Figure 1, the higher the density of the material, the brighter the color. Thus, the predominantly water-filled fluid inclusions look darker than the denser enclosing fluorite matrix. Any dense base metal-bearing accidental mineral inclusions contained within fluid inclusions should therefore appear as highly contrasting bright spots within the fluid inclusions. Thus, to identify metal-bearing accidental mineral inclusions, a filter was applied with the imaging software while scanning the image slices to identify any anomalously bright pixels within the image relative to a background threshold value. Any anomalously bright pixels identified would be inspected manually to test for a morphology that is consistent with a mineral grain.

None of the 85 fluid inclusions analyzed in the present pilot study showed any evidence of containing accidentals. These preliminary results suggest that either at least some of the high fluid inclusion metal contents reported by Pelch et al. (2015) for the Illinois-Kentucky district genuinely represent dissolved solute in aqueous solution in the fluid inclusions, or that if any accidentals existed in the fluid inclusions analyzed, then they were smaller than about 40 nm in diameter. However, before any conclusions about the occurrence of accidentals in Illinois-Kentucky fluid inclusions can be drawn with confidence, more fluid inclusions from a wider swath of the paragenetic sequence must be analyzed. Moreover, before any broader conclusions can be drawn about sediment-hosted base metal deposits generally, a greatly expanded fluid inclusion survey must be conducted spanning multiple samples from multiple deposits. Such a survey should also include sphalerite, the main target of numerous previous sediment-hosted base metal fluid inclusion studies, which reported Pb-rich fluid inclusions. Nonetheless, the present pilot study shows that fluid inclusions can be imaged successfully at nanometer-scale resolution using synchrotron nano-CT in minerals with low enough X-ray absorbance. The large (nearly two-fold) density contrast between sphalerite and galena means that galena accidentals should be clearly visible within a sphalerite host, though the higher X-ray absorbance of sphalerite compared to fluorite means that sphalerite grains should be no larger than about 40 µm in order to be imaged effectively by synchrotron nano-CT.

REFERENCES

Appold, M.S. (2021) Applications of fluid inclusions to studies of sediment-hosted base metal ore deposits: case studies from the central U.S.A. and Brazil, Mineralogical Association of Canada, Topics in Mineral Sciences 49, 47-72.

Pelch, M.A., Appold, M. S., Emsbo, P., Bodnar, R. J. (2015) Constraints from fluid inclusion compositions on the origin of Mississippi Valley-type mineralization in the Illinois-Kentucky district, Economic Geology 110, 787-808.

Roedder, E. (1984) Fluid inclusions, Reviews in Mineralogy 12, 27.

Yao, J.M., Chen, H.Y., Tian, Y.C., Song, W.L., and Zhu, S.Y. (2015) Three-dimensional imaging of a single fluid inclusion in sphalerite by nano X-ray tomography, Ore Geology Reviews 71, 116-120.

Melt inclusions in Catalina 008: Studying carbonaceous chondrite from Atacama Desert with Raman Spectroscopy

Claudia S. ARAVENA-GONZÁLEZ[1], Daniel MONCADA[2], Rodrigo MARTÍNEZ[3].

[1] *Depto de Geología, Universidad de Chile;*
[2] *Institution for Second Author (if required) – Calibri 10-point Italic font*
[3] *Museo del Meteorito, San Pedro de Atacama, Chile*
E-mail: claudia.aravena@ug.uchile.cl

Catalina 008 is a primitive carbonaceous chondrite Ornans type, distinguished by small chondrules and refractory inclusions (<0.2 mm) occupying about half the volume of the rock. This meteorite was found by R. Martínez in 2011 in the Atacama Desert, a private collector who founded the Meteorite Chilean Museum situated in San Pedro de Atacama (Meteoritical Bulletin Database, 5 July 2022). Since its discovery, this chondrite was studied by different researchers because of its low degree of aqueous alteration, resulting in an excellent sample for searching for volatiles and sensitive molecules.

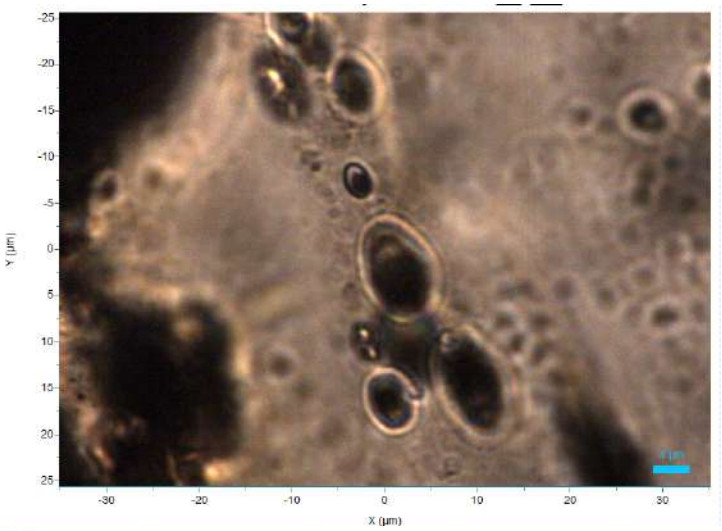

Figure 1. Fragment of olivine with melt inclusions assemblages wich reveal bubbles (in 20x resolution).

According to Gilmour I. et al. (2003), it's possible to trace different forms of carbon like CO2, amino acids, and graphite, among others. Adding the fact of some works like Bonal L. et al. (2016) report the presence of D and G bands that are interpreted as polyaromatic carbon matter in the matrix of Ornans-type carbonaceous chondrites and the preliminary results of this research confirmed the presence of these bands in some melt inclusions (Aravena González, C. S. (2019)), motivates us to continue searching these molecules in melt inclusions, expecting to acquire more data that will allow us to understand their behavior.

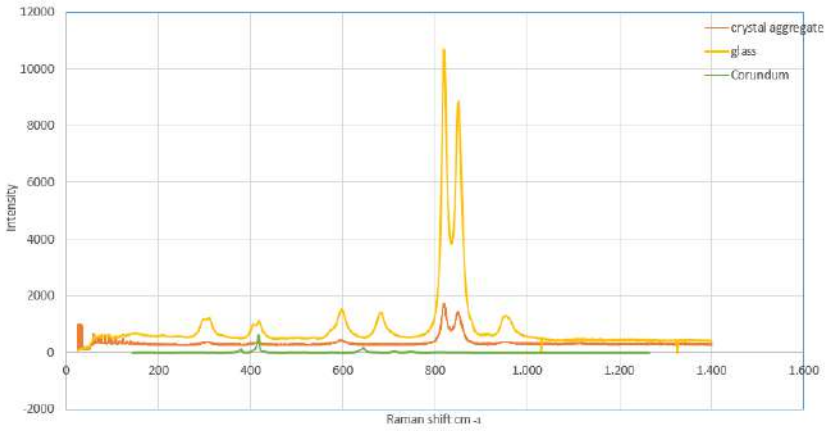

Figure 2. Spectra obtained from glassy phase (in yellow) and crystal aggregate (in orange), comparing strong peaks with corundum spectra (in green).

Using the equipment at the University of Chile (Plaza Ercilla #803, Santiago de Chile), we found melt inclusions in some fragments of olivine minerals, exploring this sample in a polished thin section. We selected melt inclusion assemblage primaries and several of them resulted to have different phases (like bubble, glass, and crystals aggregates possibly of carbon).

Raman spectroscopy was the proposal for analyzing each phase of melt inclusions present, thanks to its high sensitivity to structure and bonding within

carbonaceous molecules. Comparing each spectrum obtained in the Lab-Ram Uchile we reviewed differences that suggest variation in compositions with the host and in this way, obtained clues about the liquid that formed it.

Considering the primary liquid condensation model, proposed by Varela M. E. et al. (2018) and their analyses in chondrules of Olivine, we expected to obtain spectra with characteristic peaks of minerals like Quartz, Plagioclase, Orthoclase, Corundum, and Hypersthene.

The spectra obtained will be present in this work revealing the phases interpreted by the presence of strong characteristic peaks, using RRUFF database and based on Frezzotti M. L. et al. (2012), to discuss possible meanings concerning formation theories of olivine chondrules in Ornans type carbonaceous chondrites.

REFERENCES

Aravena González, C. S. (2019). Inclusiones vítreas en condritos carbonáceos del Desierto de Atacama, Región de Antofagasta, Chile.

Bonal, L., Quirico, E., Flandinet, L., & Montagnac, G. (2016). Thermal history of type 3 chondrites from the Antarctic meteorite collection was determined by Raman spectroscopy of their polyaromatic carbonaceous matter. *Geochimica et Cosmochimica Acta*, *189*, 312-337.

Frezzotti, M. L., Tecce, F., & Casagli, A. (2012). Raman spectroscopy for fluid inclusion analysis. *Journal of Geochemical Exploration*, *112*, 1-20.

Gilmour, I. (2003). Structural and isotopic analysis of organic matter in carbonaceous chondrites. Treatise on geochemistry, 1, 711.

Meteoritical Bulletin Database, 5 July 2022.

Varela, M. E., & Zinner, E. (2018). Unraveling the role of liquids during chondrule formation processes. *Geochimica et Cosmochimica Acta*, *221*, 358-378.

Halite fluid inclusions: a gateway to atmospheric oxygen levels and shallow marine environments in deep time

Nigel JF BLAMEY[1], U. BRAND[2], A. LEFEBVRE[1], A. MORRISON[1]

[1] *Dept. Earth Sciences, University of Western Ontario, Canada;*

[2] *Dept. Earth Sciences, Brock University, Canada*

E-mail: nblamey2@uwo.ca

It has been a goal of scientists to quantify Earth's atmospheric oxygen level in the geologic record to help determine when animal life evolved. Detrital pyrite and uraninite in Archean sediments provide good evidence for an anoxic atmosphere at that time whereas the confirmation of the first free oxygen in the atmosphere has been a challenge. Modelling by Bob Berner offered a good first estimate and the subsequent use of redox-sensitive elements (RSEs) have helped to infer a level of confidence, albeit that the error was two orders of magnitude (Lyons et al., 2014). Metal isotopes have gained popularity recently despite the lack of a calibration against modern environments. None of these approaches used direct analytical methods. However, Blamey et al. (2016) provided the first direct measurements of atmospheric oxygen in the Precambrian from halite-hosted fluid inclusions, giving quantitative measurements of ~11% pO_2. Halite is not ubiquitous in the geologic record but its presence confirms that brines were evaporating in contact with Earth's atmosphere. This allows through the formation of fluid inclusions for ambient temperatures and atmospheric bubbles to record conditions at the Earth's surface.

Halite for investigation was obtained from drill core. Material was investigated using the 7-point protocol presented by Blamey and Brand (2019) and includes: hand specimen examination; petrographic examination; microthermometry; gas analysis; trace element analysis; H and O isotopic analysis; Ar isotopic analysis; and Sr isotopic analysis. Hand specimen is invariably the first-pass test whereby one inspects the core for primary or secondary halite. In hand examination, displacive halite is easily identified and the material rejected. Petrographic examination allows the researcher to identify primary fluid inclusion trails and corresponding square-shaped fluid inclusions, good evidence for primary halite. Zones of secondary fluid inclusions are avoided and these inclusions usually present themselves as rounded, lacking the square shape. Microthermometry offers not only a measurement of fluid inclusion trapping temperatures but can also be used as a screening tool to discriminate primary from diagenetic halite based on an approximate 50° Celsius cutoff. Inclusions relating to diagenesis typically homogenize above 50° Celsius. Quantitative fluid inclusion gas analysis by mass spectrometry is a direct analytical method that measures the following volatile species: H_2, He, CH_4, H_2O, N_2, O_2, Ar and CO_2. Modern halite is used to validate the current atmospheric gas ratios, thus giving confidence to measurements made on ancient halite inclusions. The $^{40}Ar/^{36}Ar$ isotopic composition of modern atmosphere is 295 yet measurements of ancient halite inclusions range from about 300 to >900. The elevated $^{40}Ar/^{36}Ar$ results are attributed to radiogenic Ar* produced by the decay of ^{40}K. If contamination by modern atmosphere is suspected, then $^{40}Ar/^{36}Ar$ ratios will match Modern, which is not the case (see Blamey & Brand, 2019). The δ^2H and $\delta^{18}O$ of the fluid inclusion aqueous phase confirm the source of halite as being either marine (isotopically heavy) or continental (isotopically light) and therefore provide information about the paleo environment. The Br content of halite also confirm whether the fluid source was continental versus marine with Br >100 ppm confirming continental sources in contrast to <100 ppm being typical of marine halite.

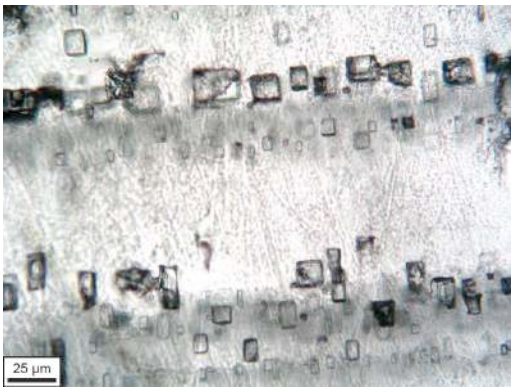

Figure 1. Primary fluid inclusion trails hosted in halite. Note the vapor-dominated inclusions in the bottom left.

The atmospheric oxygen level during the Phanerozoic has not been constant (see Brand et al., 2021; Steadman et al., 2020) (see Fig. 2). Modeling and trace element analysis suggests that Earth's atmospheric oxygen levels were highest in the Permian whereas gas analyses reported by Blamey et al. (2016) give 25% pO_2 during the Cretaceous. To address this discrepancy, a high-resolution study is required. The limitation of our method is finding primary halite in the geological record, the problem being that halite precipitation is not continuous. However, measurements from halite hosted fluid inclusion gases are correlated with some redox-sensitive elements (RSE's), the first attempt reported in Steadman et al. (2020). Correlation with other approaches will be valuable to resolve questions on whether atmospheric oxygen drove the evolution of animal life. Collaboration with other scientists can also help answer during what time intervals the oceans were redox stratified? The future looks very promising to answer several geological questions about the evolution of Earth's atmosphere, biosphere and role of oxygen in several ore deposit styles.

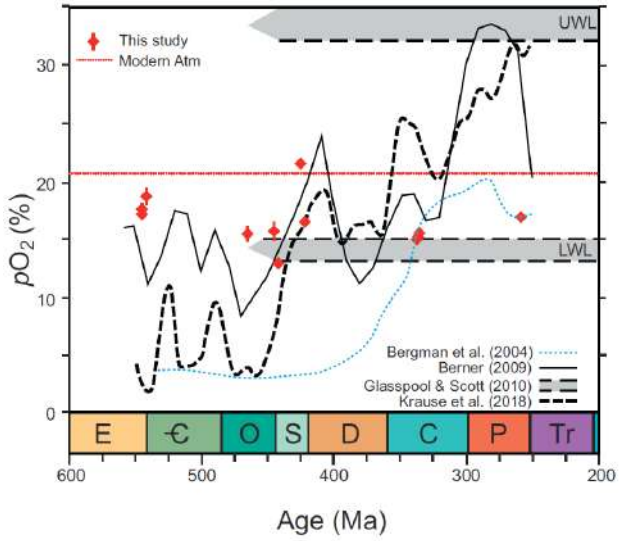

Figure 2. Comparison between halite gas measurements versus some other approaches (Brand et al., 2021).

REFERENCES

Blamey, N.J.F., et al. (2016) Paradigm shift in measuring Neoproterozoic atmospheric oxygen, Geology 12, 34-56.

Blamey, N.J.F., and Brand, U. (2019) Atmospheric gas in modern and ancient halite fluid inclusions: A screening protocol, Gond. Res. 69, 163-176.

Brand, U., et al. (2021) Atmospheric oxygen of the Paleozoic, Ear.-Sci. Rev. 216, 103560.

Lyons, T.M., et al. (2014) The rise of oxygen in Earth's early ocean and atmosphere, Nature 506, 307–315.

Steadman, J.A., et al. (2020) Evidence for elevated and variable atmospheric oxygen in the Precambrian, Precamb. Res. 343, 105722.

Temporal Evolution of Fluid on a High-sulfidation Hydrothermal System Related to Alkalic Magmatism-Silver Pond Lawyers Property, Toodoggone District, North-Central British Columbia

Sinan CANBULAT[1], Matthew Steele-MacInnis[1], Pilar Lecumberri-Sanchez[1], Pascal Voegeli[1]
[1]*Department of Earth and Atmospheric Sciences, University of Alberta, Edmonton, Alberta*
E-mail: canbulat@ualberta.ca

The Toodoggone district consists of Upper Triassic to Lower Jurassic Hazelton Group volcanic and sedimentary rocks, which unconformably overlap submarine island-arc volcanic and sedimentary rocks of the Lower Permian Asitka Group and Middle Triassic Takla Group (Duuring et al., 2009a). The Toodoggone district hosts several precious and base-metal deposits, including Baker, Cheni, Shasta, and Kemess mines. The district has been considered a high-priority exploration area with discovery potential. The Lawyers property is the area of the historical Cheni mine, which is located in the central region of the Toodoggone district. The Lawyers system is a well-maintained epithermal system hosting Au-Ag deposition. Whereas the Lawyers property depicts a typical low sulfidation epithermal system with narrow multiphase quartz-carbonate, quartz-adularia, quartz-sulfide vein, stockwork, and hydrothermal breccia zones, the Silver Pond exhibits several characteristics of high sulfidation style epithermal systems (Duuring et al., 2009a; Voegeli and Lecumberri-Sanchez, 2022). In the Silver Pond system, the condensation of magmatic gas snuggling into groundwaters triggers the disproportion of SO_2, with occurring H_2SO_4 and H_2S, which is a highly acidic solution (pH<1; Sillitoe, 1973; Arribas, 1995; Voegeli and Lecumberri-Sanchez, 2022). Sulfate, especially barite, minerals are abundant in the veins. Additionally, (Duuring et al., 2009a; Diakow et al., 1991, 1993) classified the Silver Pond as a high sulfidation epithermal system since it comprises vuggy quartz with argillic-advanced argillic alteration assemblage (dickite–quartz±natroalunite+diaspore+topaz) as well as Griz-Sickle and Al deposit areas.

Dacite and dacitic tuff, which are intensely altered, are primary host rocks in the Silver Pond epithermal system, while the dominant rocks of the Toodoggone district are latite to dacite (Diakow et al., 1991; Bouzari et al., 2019; Voegeli and Lecumberri-Sanchez, 2022). However, high sulfidation epithermal systems in the Toodoggone district (e.g., Silver Pond, Al, Griz-Sickle, Pil South, Nub West) are range in age from 200 to 188 Ma, thereby coinciding with the 202 to 197 Ma syenitic porphyry event and the earlier stages of Toodoggone volcanism and recommending a possible genetic linkage between syenitic-alkalic plutonism, porphyry mineralization, high-sulfidation epithermal mineralization and volcanism (Duuring et al., 2009b). Low-sulfidation epithermal Au-Ag mineralizations (e.g., Shasta, Baker, Lawyers, Wrich Hill) are mainly hosted by Takla Group as well as Toodoggone Formation rocks and range in age from 192 to 168 Ma. (Diakow et al., 1991), which overlap with the latest phase of felsic dike emplacement, volcanism, and fault-block subsidence at around 185 Ma.

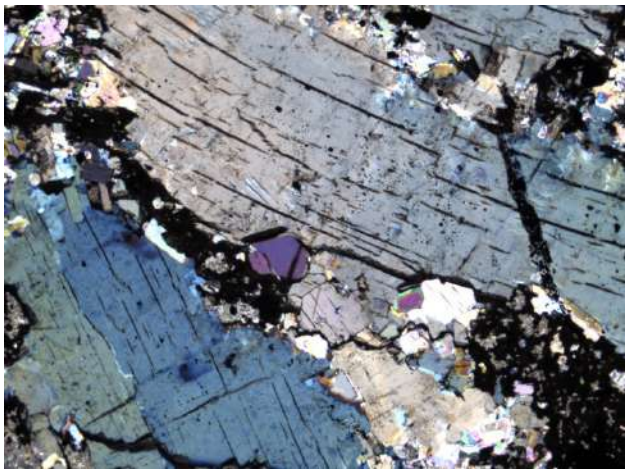

Figure 1. Sulfate minerals, tabular barite crystals in the vein. (5X, XPL)

Te (Telluride), Se (Selenide), and Tl (Thallium) are jointly reported as trace minerals associated with gold in metallogenic belts and areas by researchers (Ciobanu et al., 2006). The elemental association Au-Te-Bi-Se can be considered a magmatic signature given by these elemental associations with other chalcophile elements because of the widespread presence of Te and Se in Archean Au-quartz veins (Ciobanu et al., 2006). Especially, epithermal gold-telluride deposits are often related to alkaline magmatism (e.g., around the Pacific Rim, Fiji) (Ciobanu et al., 2006). It was reported that the Silver Pond has at least Se (up to 24000 ppm) and Tl (up to 1200 ppm) contents based on depth via drill core samples (Voegeli and Lecumberri-Sanchez, 2022).

A high concentration of Ba or barite ($BaSO_4$) crystals (tabular) and some rare earth elements (REE) can reflect the alkalic parental magmas, which can be confined as a deep intrusion (Gultekin et al., 2002). Gold-barite veins were reported in the Toodoggone district, especially for Al high-sulfidation epithermal deposits (Diakow et al., 1991), and barite has a strong affinity with gold in the veins and breccias (Diakow et al., 1993). There have not been any recorded relations between barite ($BaSO_4$) and potential/promising gold (Au) forming in the sense of the Silver Pond high sulfidation epithermal system.

The main objective of this study is to determine the temporal fluid evolution of the Silver Pond high-sulfidation epithermal deposit by investigating whether there is a relationship between alkalic magmatism and any ore, mainly gold, promising stage in detail since the veins involve sulfate, especially barite-anhydrite crystals (Figure 1). Fluid mixing (meteoric and magmatic) and deep circulation of meteoric water are widely accepted by researchers with regard to ore deposition mechanism and vectoring by cooling or boiling (Hedenquist and Hanley, 1985; Cooke and Bloom, 1990) although they have slightly been mentioned for the Silver Pond system (Voegeli and Lecumberri-Sanchez, 2022). Nevertheless, a bunch of veins consist of aqueous liquid-rich (Type 1) and aqueous vapor-rich (Type 2) fluid inclusions together in the same mineral, which can be a robust indicator of boiling. Consequently, the Silver Pond high-sulfidation system needs further investigations. It should be focused on comprehending temporal fluid evolution, potential gold forming, and association of any alkalic contribution from the deeper part of the crust.

The next analyses involving microthermometry studies, Raman spectorscopy and Scanning Electron Microscope (SEM) will be fulfilled as fitting for the purpose of the study. Fluid inclusions need further investigations to reach consistent results regarding fluid evolution and fluid flow, considering pH, salinity, gas content, heating-freezing experiments via microthermometry and Raman spectroscopy. Additionally, SEM will be crucial to identify Au from the other ore minerals by which backscattered electrons (BSE) and distinguish chemical differences and anomalies by energy dispersive spectroscopy (EDS).

REFERENCES

Voegeli, P. and Lecumberri-Sanchez, P. (2022) Spectral and geochemical characterization of the Silver Pond argillic-advanced argillic alteration lithocap, Lawyers property, Toodoggone district, north-central British Columbia, Geoscience BC Summary of Activities 2022-01 12, 21-38.

Bouzari, F. et al. (2019) An exploration framework for porphyry to epithermal transitions in the Toodoggone mineral district (94E), Geoscience BC, Report 2019-08 and MDRU Publication 424, 1-105.

Duuring, P. et al. (2009a) Examining potential genetic links between Jurassic porphyry Cu-Au±Mo and epithermal Au±Ag mineralization in the Toodoggone district of North-Central British Columbia, Canada, Mineralium Deposita 44, 463-496.

Duuring, P. et al. (2009b) Magmatic and structual controls on porphyry-style Cu-Au-Mo mineralization at Kemes South, Toodoggone District of British Columbia, Canada, Mineralium Deposita 44, 435-462.

Ciobanu, C. L. et al. (2006) Telluride and selenide minerals in gold deposits – how and why?, Mineralogy and Petrology 87, 163-169.

Gultekin, A. H. et al. (2003) Geology, mineralogy and fluid inclusion data of the Kizilcaoren fluorite-barite-REE deposit, Eskisehir, Turkey, Journal of Asian Earth Sciences 21, 365-376.

Aribas, A. (1995) Characteristics of high-sulfidation epithermal deposits, and their relation to magmatic fluid, Mineralogical Association of Canada, Short Course 23, 419-454.

Diakow, L. J. et al. (1993) Geology of the Early Jurassic Toodoggone Formation and Gold-Silver Deposits in the Toodoggone River Map Area, Northern British Columbia, Geological Survey Branch 86, 1-72.

Diakow, L. J. et al. (1991) Jurassic Epithermal Deposits in the Toodoggone River Area, Northern British Columbia: Examples of Well-Preserved, Volcanic-Hosted, Precious Metal Mineralization, Economic Geology 86, 529-554.

Cooke, D.R. and Bloom, M.S. (1990) Epithermal and subjacent porphyry mineralization, Acupan, Baguio District, Philippines: a fluid-inclusion and paragenetic study, Journal of Geochemical Exploration 35, 297-340.

Hedenquist, J.W and Henley, R.W (1985) The importance of CO_2 on freezing point mesurements of fluid inclusions: evidence from active geothermal systems and implications for epithermal ore depoisition, Economic Geology 80, 1379-1406.

Sillitoe, R.H. (1973) The tops and bottoms of porphyry copper deposits, Economic Geology 68, 799-815.

Factors controlling the formation of unconformity-related uranium deposits in the Proterozoic Athabasca Basin – insights from fluid inclusion studies

Guoxiang Chi[1], Haixia Chu[2], Morteza Rabiei[1], Eric Potter[3], Duane Petts[3], Daniel Ferguson[1]

[1]*Department of Geology, University of Regina*

[2]*China University of Geosciences (Beijing)*

[3]*Geological Survey of Canada (Ottawa)*

E-mail: Guoxiang.chi@uregina.ca

The Proterozoic Athabasca Basin in Canada hosts a large number of high-grade and large-tonnage uranium deposits, several of which contain > 100 Mt U_3O_8 with average grades between 15 wt.% and 20 wt.% U_3O_8 (~ 100,000 times enrichment over average crustal abundance). These deposits, generally located near the unconformity between the basin and the basement and spatially associated with reactivated basement faults, are referred to as unconformity-related uranium (URU) deposits, even though some of the orebodies may extend up to 1 km below the unconformity surface. The URU deposits were once thought by some researchers to be related to paleo-weathering associated with the unconformity, but the fact that the mineralization is associated with basement faults crosscutting the unconformity, plus fluid inclusion studies indicating temperatures in the range of 110° to 220°C, points to a hydrothermal rather than supergene origin. After over four decades of study, a 'diagenetic-hydrothermal' mineralization model is generally accepted, in which oxidizing basinal brines reacted with reducing basement lithologies (especially graphite-rich zones) or reducing fluids derived from the basement, and precipitated uraninite at the redox front near the unconformity (Pagel, 1975; Kotzer and Kyser, 1995; Derome et al., 2005; Richard et al., 2011, 2016).

However, the factors controlling the URU mineralization are still not fully known, as geological settings favorable for uranium mineralization, according to the diagenetic-hydrothermal model, appear to be present throughout the basin yet deposits only occur in localized areas. Unsolved problems related to the genesis of the URU deposits, which may be linked to questions regarding the factors controlling mineralization, include whether the URU mineralization took place at deep-burial (> 5 km; Pagel, 1975) or relatively shallow (< 3km; Chi et al., 2018) conditions, whether the uranium was mainly derived from the basin (e.g., Kotzer and Kyser, 1995) or from the basement (e.g., Richard et al., 2016), and what drove circulation of the large amounts of fluids required for formation of such high-grade deposits. Like in the establishment of the diagenetic-hydrothermal model, fluid inclusion studies can play an important role in addressing these problems, as demonstrated by some recent studies of fluid inclusions.

Microthermometric and LA-ICP-MS studies of fluid inclusions in quartz overgrowths from sandstones of the Athabasca Basin reveal that H_2O-NaCl-$CaCl_2$ brines (ranging from Na- to Ca-dominated varieties), which are rich in uranium (up to 27 ppm U), are widespread within the basin (Chu and Chi, 2016; Chi et al., 2019). The microthermometric and compositional data of these fluid inclusions largely overlap with those found within the URU deposits (Richard et al., 2016), suggesting that the uranium in the deposits may have been mainly derived from the sediments in the basin. Furthermore, the uniform distribution of fluid inclusion microthermometric data across different stratigraphic levels indicates strong circulation of basinal fluids within the basin, possibly driven by fluid convection. This fluid flow mechanism, facilitated by high geothermal gradients as imposed by the shallow-burial model (Chi et al., 2018) and previously proposed based on numerical modeling, is thus further supported by the fluid inclusion data.

Fluid inclusion studies from URU (Chi et al., 2014; Wang et al., 2018; Rabiei et al., 2021 and in review; Ferguson et al., in prep.) and related REE deposits (Rabiei et al., 2017) suggest that fluid boiling occurred during mineralization, as manifested by the coexistence of vapor- and liquid-dominated fluid inclusions within individual fluid inclusion assemblages (FIAs). However, even under the elevated geothermal gradients in the shallow-burial conditions, boiling is impossible unless the fluid pressure is momentarily lowered below the hydrostatic value. This condition may be episodically created by seismic events during reactivation of the basement faults, which provided

another driving force of fluid flow for the URU mineralization. Furthermore, chemical changes (e.g., pH values) related to fluid boiling may provide another mechanism for ore precipitation in addition to redox reactions.

In summary, our recent fluid inclusion studies have provided new insights on the factors controlling the formation of the URU deposits in the Athabasca Basin. Uranium may have been derived from the sediments within the basin and uraniferous fluids were widespread across the basin, and thus uranium mineralization is possible underneath the whole basin, as long as other conditions (focused fluid flow and availability of reducing agents) were met. The homogeneity of fluid inclusion compositions across the basin suggests that fluid convection is an important mechanism of fluid flow within the basin, which may have facilitated uranium extraction from basin sediments. Fluid boiling, as indicated by fluid inclusion assemblages, implies that the mineralization may be related to episodic fracturing along basement faults, which provides another driving force of fluid flow and explains why the URU deposits are associated with reactivated basement faults.

REFERENCES

Chi, G., Liang, R., Ashton, K., Haid, T., Quirt, D., and Fayek, M. (2014) Evidence of fluid immiscibility from uranium deposits in northern Saskatchewan and Nunavut and potential relationship with uranium precipitation. GAC-MAC Abstracts, v. 37, p. 57.

Chi, G., Chu, H., Petts, D., Potter, E., Jackson, S., Williams-Jones, A.E. (2019) Uranium-rich diagenetic fluids provide the key to unconformity-related uranium mineralization in the Athabasca Basin. Scientific Reports, (2019) 9: 5530.

Chi, G., Li, Z., Chu, H., Bethune, K.M., Quirt, D.H., Ledru, P., Normand, C., Card, C., Bosman, S., Davis, W.J., Potter, E.G. (2018) A shallow-burial mineralization model for the unconformity-related uranium deposits in the Athabasca Basin. Economic Geology, v. 113, p. 1209-1217.

Chu, H., and Chi, G. (2016) Thermal profiles inferred from fluid inclusion and illite geothermometry from sandstones of the Athabasca basin: Implications for fluid flow and unconformity-related uranium mineralization. Ore Geology Reviews, v. 75, p. 284-303.

Derome, D., Cathelineau, M., Cuney, M., Fabre, C., Lhomme, T., and Banks, D.A. (2005) Mixing of sodic and calcic brines and uranium deposition at McArthur river, Saskatchewan, Canada: A Raman and Laser-induced breakdown spectroscopic study of fluid inclusions. Economic Geology, v. 100, p. 1529-1545.

Kotzer, T., and Kyser, T. (1995) Petrogenesis of the Proterozoic Athabasca Basin, northern Saskatchewan, Canada, and its relation to diagenesis, hydrothermal uranium mineralization and paleohydrogeology. Chemical Geology, v. 120, p. 45-89.

Pagel, M. (1975) Détermination des conditions physico-chimiques de la silicification diagénétique des grès Athabasca (Canada) au moyen des inclusions fluides. Comptes Rendus Académie Sciences Paris, v. 280, p. 2301-2304.

Rabiei, M., Chi, G., Normand, C., Davis, W.J., Fayek, M., Blamey, N. (2017) Hydrothermal REE (xenotime) mineralization at Maw Zone, Athabasca Basin, Canada, and its relationship with unconformity-related uranium deposits. Economic Geology, v. 112, p. 1483-1507.

Rabiei, M., Chi, G., Potter, E.G., Tschirhart, V., MacKay, C., Frostad, S., McElroy, R., Ashley, R., McEwan, B. (2021) Fluid evolution along the Patterson Lake corridor in the southwestern Athabasca Basin: constraints from fluid inclusions and implications for unconformity-related uranium mineralization. Geochemistry: Exploration, Environment, Analysis, v. 20, geochem2020-029.

Richard, A., Banks, D., Mercadier, J., Boiron, M., Cuney, M., and Cathelineau, M. (2011) An evaporated seawater origin for the ore-forming brines in unconformity-related uranium deposits (Athabasca basin, Canada): Cl/Br and δ^{37}Cl analysis of fluid inclusions. Geochimica et Cosmochimica Acta, v. 75, p. 2792-2810.

Richard, A., Cathelineau, M., Boiron, M.-C., Mercadier, J., Banks, D.A., and Cuney, M. (2016) Metal-rich fluid inclusions provide new insights into unconformity-related U deposits (Athabasca basin and basement, Canada). Mineralium Deposita, v. 51, p. 249-270.

Wang, K., Chi, G., Bethune, K.M., Li, Z., Blamey, N., Card, C., Potter, E.G., Liu, Y. (2018) Fluid P-T-X characteristics and evidence for boiling in the formation of the Phoenix uranium deposit (Athabasca Basin, Canada): implications for unconformity-related uranium mineralization mechanisms. Ore Geology Reviews, v. 101, p. 122-142.

The Timing and Setting of Copper mineralization in the Timna Igneous Complex, Northernmost Arabian-Nubian Shield

Alon Elhadad[1], Yevgeny Vapnik[1], Bar Elisha [1], Itai Haviv[1], Yaron Katzir[1]
[1]*Ben-Gurion University of the Negev, Beer-Sheva, Israel.*
E-mail: alonelh@post.bgu.ac.il

Copper mineralization in the northernmost Arabian-Nubian Shield (ANS) mostly occurs within ring dyke complexes of the southern Sinai Peninsula, Egypt. It is marginally economic and attributed to porphyry copper systems related to calc-alkaline granites and meso- to epithermal systems (Mamedov et al., 2014). These intrusions mark the tectono-magmatic transition from East African collisional (670-630 Ma; Be'eri-Shlevin et al, 2009) to post collisional setting (620-590 Ma), during which magmatism changed from calc-alkaline, mostly I-type granites to alkaline A-type granites. Copper mineralization in the Timna Igneous complex (TIC) of southern Israel presumably occurred during equivalent tectono-magmatic transition, but the absence of primary sulfides makes reconstruction of the setting and timing of primary copper mineralization difficult (Würzburger, 1967; Charrach 1976). In the TIC, mineralized felsic to intermediate rocks are characterized by the abundance of secondary Cu-sulfides (chalcocite and covellite) that were thought to precipitate from low-temperature (150-170^{o}C) hydrothermal fluids, and later altered to malachite, atacamite and chrysocolla. Similar copper assemblages occur in impregnations, veins and breccias within the overlying, Cambrian sandy-dolomite Timna Fm., forming an economic ore body exploited until recently (Segev and Sass, 1989). Thus, the scarce copper mineralization within the TIC may either originate from basinal brines mobilizing copper along the igneous basement – sedimentary cover unconformity or represent altered late magmatic-hydrothermal mineralization. The only means to determine whether primary ore-forming fluids were truly magmatic or basinal in origin is by the study of fluid inclusions (FI) trapped in gangue minerals.

The major Cu-bearing assemblages are hosted by relatively fresh alkaline quartz porphyry (QP) stock, an extensively altered quartz monzonite (QM), a moderately mineralized calc-alkaline porphyritic granite (PG) and uncommon quartz veins (QV). FIs are trapped in quartz phenocrysts in PG and QP and in interstitial quartz in QM. Cu-bearing minerals are associated with aggregates of unusually coarse-grained zircon and rutile (100-500μm) in the QP, providing a rare opportunity to track ore evolution in time. In addition to the dominant secondary assemblage, as found in all samples, QP samples hold relicts of pyrite, pyrrhotite, galena, sphalerite and chalcopyrite sheltered in goethite as pseudo-secondary and primary inclusions hosted in quartz phenocrysts, and in seemingly "miarolitic" quartz (Fig. 1a, b).

FI types include: (1) aqueous liquid-rich with a small vapor bubble (10-15 vol.%; Fig 1c.i) found in all samples as secondary assemblages; (2) CO_2 vapor-rich inclusions with a small aqueous liquid rim (5-10 vol.%; Fig 1c.iii); (3) CO_2 vapor-rich with a carbonic liquid phase (10-15 vol.%) and a small aqueous liquid rim (5-10 vol.%); an uncommon volatile phase, possibly methane is indicated by CO_2 triple point melting at temperatures of -63 to -56.6 ^{o}C. FI Types 2 and 3 are exclusive to QP samples and occur as pseudo-secondary assemblages together with scarce type 1 FIs and in association with embayments (Fig 1c); (4) halite bearing FIs with some oxide/sulfide and carbonic solid phases (~10 vol.%; Fig 1c.ii)

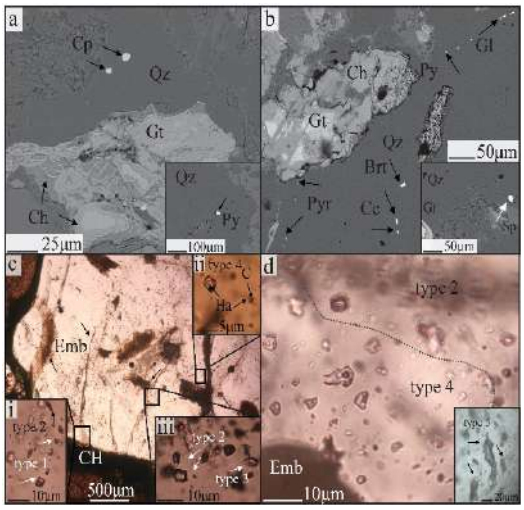

Figure 1. Quartz phenocryst in quartz porphyry sample bordering copper hydrates (CH) (a) "miarolitic" quartz, bordering goethite (Gt) and chrysocolla (Ch), hosting chalcopyrite (cp) inclusions. Inset shows primary pyrite (Py) inclusion. (b) Quartz phenocryst hosting pseudo-secondary inclusion arrays of pyrite, pyrrhotite (Pyr), chalcocite (Cc), galena (Gl) and barite (Brt). Inset shows a primary sphalerite inclusion. (c) quartz phenocryst hosting the entire FI type variety. (d) Embayment associated, immiscible pseudo secondary FIA. Inset shows type 5 FIs found in porphyritic granite sample.

found mostly in QP samples, scarcely in immiscible assemblages with type 2 FIs (Fig 1d); Type 4 FIs are sporadic and rare in PG, QM and QV; (5) exceedingly low density vapor rich inclusions found in PG, QM and QV samples (Fig 1d).

Correlation of FI petrography and microthermometry (Fig. 2) constrains three main fluid events: (1) aqueous liquid-rich, with salinity of 0-11 wt% NaCl eq., low-moderate Ths of 115-238 ^{o}C, trapped as secondary arrays in phenocryst-copper hydrate veinlet interface in QP, PG as well as in interstitial quartz in QM. (2) minor fluid immiscibility assemblage between a high salinity aqueous liquid (25-34 wt% NaCl eq. halite), with Th of 120-266 ^{o}C and CO_2 vapor decrepitating at ~290^{o}C. (3) heterogenous trapping of pseudo-secondary CO_2-vapor rich type 2 and 3 with salinity of 2-12 wt% NaCl eq. and moderate to high "apparent" Th range of 235-388 ^{o}C, and a scarce, aqueous-liquid rich with moderate salinity of 9-25 wt% NaCl eq. and overlapping Ths range of 138-270 ^{o}C.

Concordant U-Pb ages of the gangue minerals yielded slightly older cores of 610 -620 $\pm$ 5 Ma and younger rims of 605 $\pm$ 5 Ma in zircon, along with 594 $\pm$ 5 Ma rutile. U-Th/He thermochronology of rutile indicates that the rocks cooled below 230^{o}C at 580 $\pm$ 20 Ma .

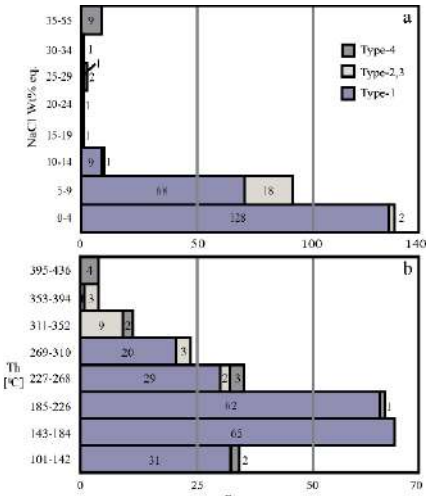

Figure 2. Fluid inclusion data. (a) Frequency distribution of salinity (NaCl Wt%. eq.). (b) Frequency distribution of homogenization temperature (Th).

The occurrence of primary sulfides and immiscible relatively high-salinity fluids, and the similarity of U-Pb ages in ore-associated zircon and rutile to the East-African crystallization ages of the TIC, suggest that copper mineralization is magmatic-hydrothermal in origin. However, the abundance of CO_2-rich fluid is not characteristic of such sulfide-bearing alkaline, A-type sub-volcanic rocks (QP) due to oxygen fugacity considerations. This may indicate a possible crustal sulfide and methane source as indicated in type 5 inclusions found in PG samples. Furthermore, the older zircon cores and their unusual size suggest them being xenocrysts, possibly derived from the I-type, calc-alkaline PG. FIAs are suggested to have been trapped during the following stages:

(1) QP Magma degassing as indicated by heterogenous trapping of CO_2-rich type 2 and 3 and moderately saline type 1 aqueous liquid-rich inclusions associated with embayments. This allowed initial metal mobilization due to increase in ligand concentrations in the residual fluids.

(2) Crystallization and major exsolution of magmatic aqueous fluids undergoing weak differentiation as indicated by uncommon immiscible FIA of high salinity type 4 and low-density type 2 FIs. Overpressure following crystallization allowed Cu-bearing fluids to mobilize to country rocks such as QM, PG, and possibly QVs during fracture propagation.

(3) Late, low salinity fluids, which may be a mixture of magmatic-hydrothermal and meteoric fluids, altered the mineralized and surrounding country rocks.

This study suggests mineralization found within calc-alkaline and alkaline complexes incorporate a significant crustal component which has yet to be indicated and may affect exploration framework.

REFERENCES

Be'eri-Shlevin et al. (2009).

Charrach, J. (1976). Geochemical Aspects of the Mineralization in the Timna Area, Southern Israel. MSc thesis, Ben-Gurion University of the Negev.

Eyal, M., Litvinovsky, B., Jahn, B. M., Zanvilevich, A., & Katzir, Y. (2010). Origin and evolution of post-collisional magmatism: coeval Neoproterozoic calc-alkaline and alkaline suites of the Sinai Peninsula. Chemical Geology, 269(3-4), 153-179.

Mamedov, E. A., Ahmed, E. S., & Chiragov, M. I. (2014). Copper–gold–sulphide mineralization associated with late Precambrian volcanic ring structures, southern Sinai, Egypt. Arabian Journal for Science and Engineering, 39(1), 273-286.

Segev, A., & Sass, E. (1989). Lithofacies and thickness control by epigenetic dissolution—the dolomitic Timna Formation, Cambrian, Southern Israel. Sedimentary Geology, 63(1-2), 109-126.

Würzburger, U. S. (1967). The occurrence of sulfides in the Timna massif and secondary copper minerals in the Timna
copper deposit, Negev (southern Israel). MSc thesis, Imperial College, London.

Fluid inclusions trapping temperatures as calibration tools in modeling sedimentary basins

Alexy ELIAS BAHNAN[1], Metzger MOMBO MOUKETO[1], Salim ALLOUTI[1], Raymond MICHELS[1], Jacques PIRONON[1]

[1]*Université de Lorraine, CNRS, GeoRessources lab, 54000 Nancy, France*

E-mail: alexy.elias-bahnan@univ-lorraine.fr

The reliable assessment of the thermal histories of sedimentary basins is often dependent on the availability of good-quality vitrinite measurements. Serving as a calibration parameter, the reflectance of vitrinite macerals can help in analyzing the thermal history of a basin. However, not all sedimentary sequences are rich in vitrinite or organic matter, especially in pre-Devonian strata where plants yielding vitrinite are absent (Allen and Allen, 2005). High hydrogen content in kerogens and aliphatic-rich vitrinite can decrease and suppress the reflectance of vitrinite leading to an underestimation of the thermal history (Carr, 2000). Also, the maturity of organic matter can be retarded by overpressure during rapid burial as vitrinite can no longer release their volatiles from their internal structure (McTavish, 1978). Issues like these are numerous yet often overlooked by geomodellers, thus rendering the thermal model risky and perhaps unreliable. Therefore, an additional calibration parameter should be used together with vitrinite to better calibrate and justify the thermal model.

The Lorraine Coal Basin (LCB) in NE France is now being considered as a potential target for coal-bed methane (CBM) exploitation, given the present-day high demand for natural gas and its relatively greener carbon footprint. The geologic history of the LCB started with successive episodes of extension-compression-transpression during the Carboniferous, extension and rhyolitic volcanism during the Permo-Triassic, gradual burial by the Late Cretaceous followed by uplift and erosion in the Paleogene until today. Of the many crucial parameters needed to estimate the quantity and quality of the potential hydrocarbon prospect is the maximum burial temperature. To this end, conventional vitrinite reflectance measurement were made available to calibrate the heat flow history. Plotted in figure 1 (black rhombs), the vitrinite show a reflectance of 0.69 % at a depth of 665m up to ~1% at a depth of 1830m. However, these values do not reproduce a thermal model that can justify the temperatures recorded in fluid inclusions (plotted as equivalent vitrinite measurements in the red triangles). This misfit is mainly due to the presence of hydrogen-rich vitrinites and exinite (spores) in the studied samples (Izart et al. 2016) which can suppress the vitrinite reflectance measurements (Car, 2000). Therefore, we present in this study a case study of using the trapping temperatures of fluid inclusions as calibration parameters, to compliment and overcome the underestimation of thermal models when based solely on vitrinite reflectance.

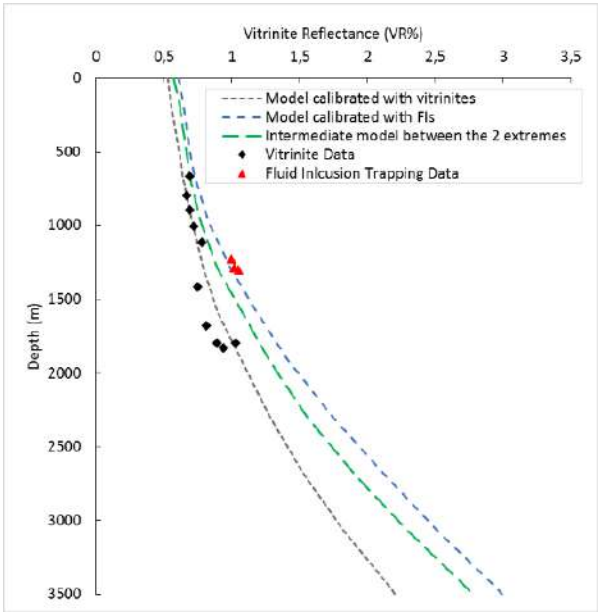

Figure 1. Vitrinite reflectance vs. depth plot showing the different thermal models calibrated using vitrinites (grey) and fluid inclusions (blue). The green model is an intermediate scenario between the grey and the blue.

Fluid inclusions assemblages (FIAs) are studied in Ankerite (Fe-rich calcite) veins from the Westphalian C formation, Saulcy well, Lorraine Basin, NE France. These samples are retrieved from a present-day depth of 1230 to 1290m. The Ankerite cements contain FIAs consisting of coexisting primary aqueous inclusions (T_h of 108°C, minimum of 100°C and a maximum of 115°C with salinities of ~ 18-20 wt% NaCl equivalent) and oil inclusions (T_h of

64 to 80°C). The co-existence of both aqueous and oil inclusions in the same FIA justifies the application of the double-isochore method to determine the trapping conditions (Roedder and Bodnar, 1980). The isochores of the aqueous phase were drawn using the Zhang and Frantz (1987) equation of state (EoS). Oil inclusion modeling was done following the Peng-Robinson (1976) EoS. Raman laser spectroscopic measurements were conducted and revealed the absence of any dissolved gases in the liquid phase. Pairs of oil and aqueous inclusions were then modeled, their isochores drawn, and their trapping T conditions were determined to be between 117°C and 128°C. The margin of error should not exceed 5% following the protocol of Bourdet et al. (2008).

Petromod 1D® was used to model the burial history of the Saulcy well. Initially, modelling was based on the vitrinite reflectance data and the maximum temperature of the Westphalian C formation, attained during the Late Cretaceous, reached 109°C. This thermal model is plotted in figure 1 (grey dashed line), as equivalent vitrinite maturity following the Sweeney and Burnham (1990) kinetic model. The heat flow in this scenario is limited to a maximum of 50 mW/m^2 during the Permo-Triassic and cools to 40 mW/m^2 by the Late Cretaceous. The Westphalian C formation in this scenario does not reach the maximum of 128°C recorded by the trapping T of fluid inclusions. We consider this scenario as a conservative estimation of the burial history and a possible underestimation of the real burial temperatures. The scenario modeled using the trapping T of FIs is plotted as the blue dashed line in figure 1. This scenario involves a Permo-Triassic heat flow of 60mW/m^2 that decreases gradually to 48mW/m^2 by the Late Cretaceous. Such a thermal history allows the Westphalian C formation to reach a maximum burial temperature of 126°C during the Late Cretaceous, in good agreement with the range of trapping temperatures of FIs. The main limitation of this heat flow scenario is that it relies only on the temperatures of a fluid event that may (or may not) be limited in time and duration. Thus, this model can be an overestimation of the equilibrium burial temperatures. To provide an intermediate model between the 2 aforementioned extremes, the thermal model in the green dashed line of figure 1 is proposed. This model can take into account some of the vitrinite reflectance values, yet allows the Westphalian C formation to reach a maximum temperature of 120°C, very close to the trapping T range of the fluid inclusions.

The case study presented in this work demonstrates how the trapping temperatures of fluid inclusions can enhance the calibration of the thermal history of any sedimentary basin. When faced with underestimated calibration parameters, in this case vitrinite, the trapping T of FIAs can provide an upper limit of the temperatures that the studied formation experienced. It remains, nonetheless, difficult to reconcile the 2 calibration parameters given the different interpretation each one carries. Fluid inclusions may resemble a fluid event of a limited duration while vitrinite reflectance reveal the accumulated thermal history. The proposed workflow here applies more robustly to cases when the studied fluid inclusions were trapped from a fluid event in thermal equilibrium with the burial conditions. Arguments need to be well-constrained as to whether or not the fluid inclusions were trapped from a hydrothermal event. If at equilibrium, then the thermal model calibrated with FIs can be justifiable. However, if the FIs were trapped from a short-lived fluid event, in disequilibrium with the burial conditions, then the thermal modeling by FIs should be used as an upper limit to the burial temperatures and an intermediate thermal scenario should be proposed.

REFERENCES

Carr, A. D. (2008) Suppression and retardation of vitrinite reflectance, part 1. Formation and significance for hydrocarbon generation, J. Pet. Geol. 23, 313-343.

Izart, A. et al. (2016) Modelling of the thermal history of the Carboniferous Lorraine Coal Basin: Consequences for coal bed methane. Int. J. Coal Geol. 168, 253-274

McTavish, R.A. (1998) The role of overpressure in the retardation of organic matter maturation. J. Pet. Geol. 21, 153-186.

Peng, D., Robinson, D.B. (1976) A New Two-Constant Equation of State. Ind. Eng. Chem. Fundam. 15, 59-64.

Sweeney, J.J., Burnham A.K. (1990) Evaluation of a simple model of vitrinite reflectance based on chemical kinetics. AAPG Bull. 74, 10, 1559 - 70.

Zhang, Y.G., Frantz, J.D. (1987) Determination of the homogenization temperatures and densities of supercritical fluids in the system NaCl-KCl-$CaCl_2$-H_2O using synthetic fluid inclusions. Chem. Geol. 64, 335-350.

The healing power of Faden quartz (Zhob District, Pakistan)

András FALL, Estibalitz UKAR
Bureau of Economic Geology, Jackson School of Geosciences, The University of Texas at Austin, Austin, Texas, USA
E-mail: andras.fall@beg.utexas.edu

The development of natural fractures can be influenced by chemically assisted fracture growth and changes to the mechanical properties of the rock and fracture networks by dissolution and precipitation reactions that occur during brittle deformation (Laubach et al., 2019). Chemical reactions can produce fracture-filling minerals that may partially to fully occlude fractures and fault zones, enhancing or degrading the capability of fractures and faults to conduct fluids (and heat). In many cases, textures of fracture-filling minerals and/or fluid inclusions trapped within them can be used to reconstruct the history of deformation and fluid geochemistry (Fall, 2021), both of which are essential for the development of hydrocarbon, water, and geothermal reservoirs and for the underground storage of CO_2, energy, (e.g., natural gas, hydrogen, water, compressed water), and waste (e.g., nuclear).

One of the most common fracture-filling minerals in the subsurface is quartz. Unlike in metamorphic environments where quartz typically fills the entire fracture (i.e., quartz veins), in diagenetic environments quartz precipitated *during* active fracture growth tends to form rims or isolated deposits that locally bridge the fracture. Crack-seal texture-bearing quartz bridges have been extensively documented in sedimentary rocks (see Fall, 2021). Similar types of cement deposits also form in hotter and deeper Alpine-type fractures (Mullis, 1975). Alpine-type synkinematic quartz bridges are well known in the world of healing crystals, and are referred to as Faden quartz owing to the milky, string-like zone passing through the core of the crystals (the *faden*, or thread in German). A quick search for "faden quartz" on the internet returns a plethora of literature informing the curious reader that due to the presence of the thread the crystals "can heal, give energy to form connection between people, and strengthen the silver chord that connects the astral self to the physical self" (e.g., www.crystalage.com), among other capabilities. Beyond the literature on placebo effects, however, genuine material describing the nature and origin of faden quartz is scarce and challenging to find. Nevertheless, mutual key words including "healing" and "connecting" point towards interacting fracturing and geochemical processes (e.g., Mullis, 1975; Ramsay, 1980; Richards, 1990; Becker et al., 2010) that can potentially explain the origin of faden quartz.

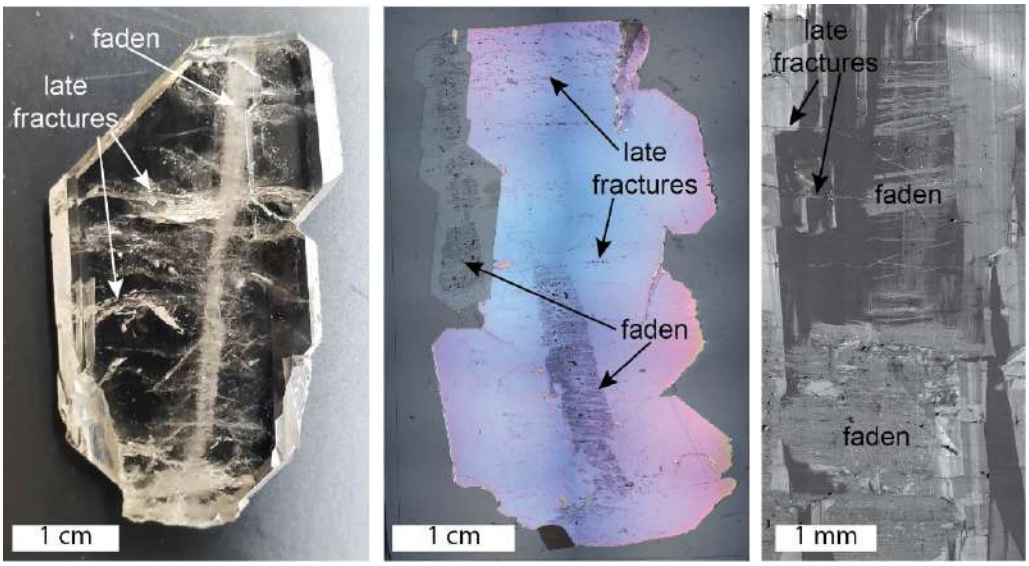

Figure 1. Left – Faden quartz showing the central thread and late microfractures; center – Transmitted light microphotograph on faden quartz showing fracture-wall parallel trails of fluid inclusions; right – SEM-CL image of faden quartz reveals fracture-wall-parallel crack-seal and clear lateral overgrowth cements that trap the FIAs.

Faden quartz localities are abundant (see Richards, 1990). Moreover, the T and P conditions at which such quartz deposits presumably form (low-temperature metamorphic grade; e.g., Ramsay and Huber, 1983; Richards, 1990) are relevant for geologic reservoirs that relay on the permeability provided by fully to partially open fractures. In order to shed light on the mechanisms, T and P conditions, and rate of faden quartz precipitation, we examined a series of crystals (Figure 1) from the Zhob District of Balochistan, Pakistan, using optical and scanning electron microscope-based cathodoluminescence (SEM-CL) and fluid inclusion microthermometry methods employed in the study of better-known diagenetic quartz bridges (Fall, 2021). Zhob faden quartz crystals range from a few millimeters to more than 10 cm in length and formed in fractures within quartzites showing pressure solution textures and minor amounts of iron oxides and chlorite. Faden quartz forms simple to complex arrays of doubly terminated crystals that are only locally attached to the wall rock. Attachment points coincide with the location of the faden thread on both sides of the fracture. The central thread, or faden, is comprised by numerous, closely spaced subparallel microfractures as revealed by SEM-CL (Figure 1) that trapped textbook examples of aqueous fluid inclusion assemblages (FIAs) parallel to the fracture walls (Figure 2). Textures show that the inclusions in the thread were trapped by the crack-seal mechanism of repeated fracturing and sealing (healing). The inclusions are two-phase at room temperature and range up to ~100 µm in size, most having negative crystal shapes. Some of the inclusions line up across adjacent microfractures (crack-seal increments), probably controlled by the crystallographic continuity of the quartz. The central thread is surrounded by late, clear euhedral quartz overgrowths with their *c*-axes at various angles with the fracture walls. The clear overgrowth is cut by late microfractures that also trapped aqueous fluid inclusions. Some of the faden are bent, presumably as a result of differential opening and/or shearing during fracture growth.

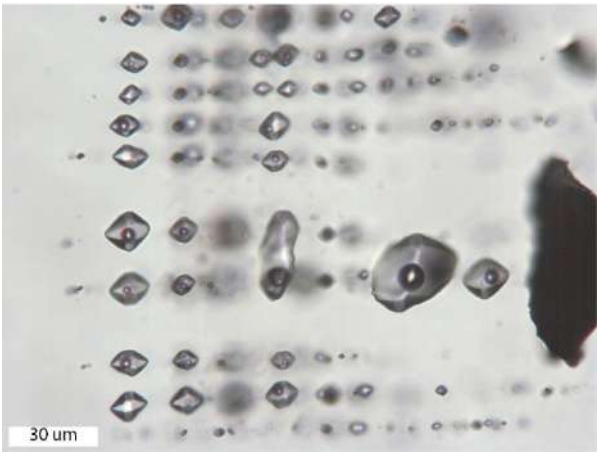

Figure 2. Photomicrograph of parallel fluid inclusion assemblages, horizontal on the image, in faden quartz.

Preliminary microthermometric data shows narrow T and salinity ranges within single crystals and across multiple generations of FIAs ranging from ~140-146°C (minimum trapping T) and 3.5-5.0 wt% NaCl equiv. in quartz-only fractures to 155-165°C and 0.0-0.5 wt% NaCl equiv. in quartz + carbonate-filled fractures. Corrected trapping T and P conditions indicate that faden fractures formed above 225°C and 1.5 kbar, corresponding to low-grade greenschist facies conditions.

A phase of synkinematic quartz growth during which the fracture was only locally filled by sparse, narrow pillars of quartz (up to a few mm) was followed by a phase of postkinematic, clear quartz growth during which several centimeters of quartz cement accumulated, resulting in a considerable reduction of fracture permeability. Microthermometric data within single and across all FIAs are the same in synkinematic faden and postkinematic clear quartz overgrowths, as well as in microfractures cutting both faden and overgrowths. Based on these narrow and consistent T ranges we conclude that the “healing” process and formation of faden quartz and similar vein fill deposits can be a rather rapid process in geologic time. Rapid accumulation of porosity occluding fracture cements at ≥200°C can be detrimental for subsurface fluid flow, and storage and production of fluids and geothermal energy, necessitating further investigation.

REFERENCES

Becker, S.P. (2010) A 48 m.y. history of fracture opening, Cretaceous Travis Peak Formation, East Texas, GSA Bull. 122, 1081-1093.

Fall (2020) Applications of fluid inclusions in structural diagenesis. Topics Min. Sci. 49, p. 17-46.

Laubach et al. (2019). The role of chemistry in fracture pattern development and opportunities to advance interpretations of geological materials, Rev. Geophys. 57, 1065–1111.

Mullis, J. (1975) Growth conditions of quartz crystals from Val d'Illiez (Valais, Switzerland), Schweiz. Mineral. Petrog. Mitt. 55, 419-429.

Ramsay, J.G. (1980) The crack-seal mechanism of rock deformation. Nature 284, 135-139.

Ramsay, J.G., Huber, M.I. (1983) The techniques of modern structural geology: Vol. 1, London, 306 p.

Richards, R.P. (1990) The origin of Faden quartz, The Min. Rec. 21, 191-201.

Characteristics of fluid inclusions and Pressure evolution in the second member of Dengying in Pengtan area, Sichuan Basin,China

Junjia Fan[1,2], Xuesong Lu[1,2], Jacques Pironon[3], Alexy Elias Bahnan[3], Xiuyan Liu[4], Xinzhi Ma[1,2], Lili Gui[1,2]

[1] *Research Institute of Petroleum Exploration and Development, Beijing 100083*

[2] *State Key Laboratory of Enhanced Oil Recovery, Research Institute Petroleum Exploration and Development, Beijing 100083*

[3] *Université de Lorraine, CNRS, GeoRessources, F-54506 Vandoeuvre-lès-Nancy, France*

[4] *Key Laboratory of Tectonic and Petroleum Resource of Educational Ministry, China University of Geoscience, Wuhan 430074, China*

The relationship between carbonate diagenesis and formation pressure evolution has become a key link in revealing large-scale natural gas charging and accumulation. Recently, major discoveries have been made in the Sinian Dengying Formation on the northern slope of the Central Sichuan Palaeohigh in the Sichuan Basin. Taking the Dengying 2 Member gas reservoir in the Penglai area as an example, this paper uses the macro and micro-observations of cores and thin slices, fluid inclusions microthemometry, laser Raman spectroscopy analysis, PVT simulation and other technical methods to clarify the paragenesis sequence of the Dengying formation and reveal the pressure evolution history of Sinian Dengying Formation. The results show that various types of inclusions are developed in the Deng 2 Member in the Pengtan area of the Sichuan Basin, including gas-liquid two-phase inclusions, single-phase methane inclusions, bitumen inclusions and mineral inclusions containing calcite(Fig.1). Dengying 2 Member reservoir has experienced multiple stages of diagenetic evolution, two stages of paleo-crude oil charging; the destruction of paleo-crude oil in the early stage, the cracking of paleo-crude oil in the late stage, and then adjust the gas reservoir distribution. Methane bearing fluids inclusions in dolomite, quartz, and fluorite reflect that the pressure system of Sinian gas reservoirs experienced six stages: normal pressure→weak overpressure→strong overpressure→extremely strong overpressure→strong overpressure→weak overpressure process, it is clear that the abnormally high pressure of the Sinian system is mainly caused by rapid burial, high temperature and cracking of crude oil. The Sinian system in the Penglai area has experienced the formation of two stages of paleo oil charging, and the existence of early bitumen indicates that the first-stage paleo-oil formed at the end of the Silurian period had been destroyed in the early Hercynian movement; The early stage of the Permian was the period of main hydrocarbon generation and accumulation of source rocks in the study area. The rapid burial of the Permian-Early Cretaceous promoted the simultaneous development of overpressure and hydrocarbon generation. The preservation of the gas reservoirs in the Penglai area is mainly related to the continuous overpressure from the Late Jurassic to the Late Cretaceous. The area with paleo-fluid overpressure in the Sinian of the Sichuan Basin may be a favorable area for future exploration and development.

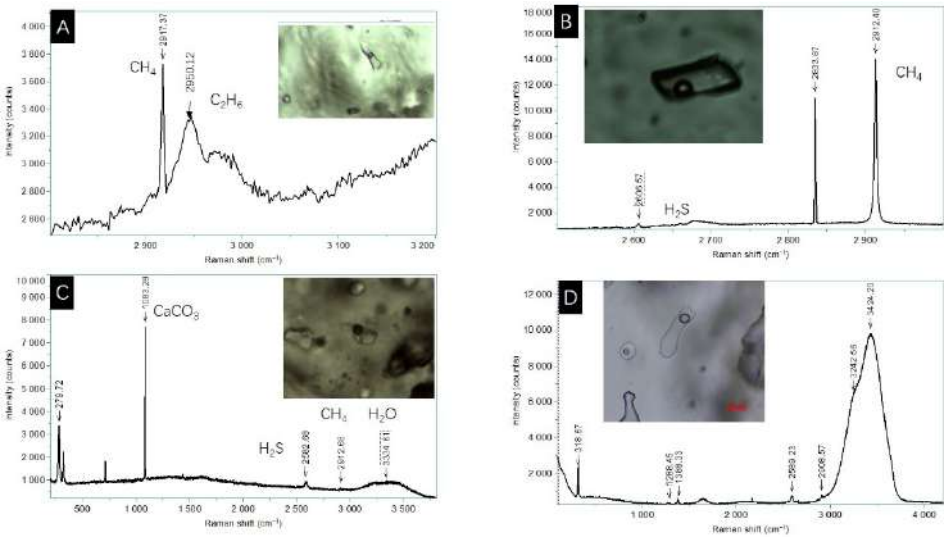

Figure 1. Different types of fluids and Raman spectral characteristics of the Sinian Dengying Formation in the Sichuan Basin.

REFERENCES

Zhu, G., A.V. Milkov, Z. Zhang, et al., Formation and preservation of a giant petroleum accumulation in superdeep carbonate reservoirs in the southern Halahatang oil field area, Tarim Basin, China. AAPG Bulletin, 2019. 103(7): 1703-1743.

Zhu, G., A.V. Milkov, J. Li, et al., Deepest oil in Asia: Characteristics of petroleum system in the Tarim basin, China. Journal of Petroleum Science and Engineering, 2020. 199(4): 108246.

Zhu, G., F. Chen, Z. Chen, et al., Discovery and basic characteristics of high-quality source rocks found in the Yuertusi Formation of the Cambrian in Tarim Basin, China. Journal of Natural Gas Geoscience, 2016: 21-33.

Worden R. H., O.N. H., and S.P. C., Can oil emplacement prevent quartz cementation in sandstones? Pet. Geosci. 4: 129-137.

J., O.M. and S.R. E., Mechanisms for generating overpressure in sedimentary basins: A reevaluation. Am. Assoc. Pet. Geol. Bull. , 1997. 81: 1023–1041.

Fluid inclusion study along the Midwest Trend, Athabasca Basin, Saskatchewan

Daniel P. Ferguson[1], Guoxiang Chi[1], Charles Normand[2], Yumeng Wang[1], Remy Chemillac[3], John Robbins[3], Patrick Ledru[3].

[1]*University of Regina*

[2]*Saskatchewan Geological Survey*

[3]*Orano Canada Incorporated*

E-mail: dpf949@uregina.ca

Midwest is a classic example of an unconformity-related uranium deposit (URU) in the Athabasca Basin. The main structural feature of the property, the Midwest Trend, is a north-northeast trending, steeply dipping fault zone rooted in graphitic pelite gneiss that has been reactivated with reverse displacement. Along the Midwest Trend characteristic features of URU have been developed including unconformity-, basement-, and sandstone-hosted mineralization, barren structure between mineralized zones, intense hydrothermal clay alteration, silica removal, and complicated hematitization and bleaching patterns. Petrographic observations of ore textures and cross-cutting relationships indicate a complex, multi-stage paragenesis characterized by an initial phase of primary mineralization followed by at least two episodes of ore remobilization. Three distinct generations of uraninite have been identified, with each generation separated by Ni-Co arsenide and sulpharsenide deposition. This sequence of mineral precipitation is consistent with geochemical reaction path modelling involving mixing between an oxidizing, U-bearing fluid and a relatively reduced Ni-Co-As bearing fluid.

A study of fluid inclusions hosted within syn- to post-ore drusy quartz was performed to determine the nature of the ore-forming and subsequent fluids. The aim of this study was to determine the salinity, composition of major, minor, and trace solutes, and P-T conditions of mineralization. Five types of fluid inclusions were found in the drusy quartz, including: (1) mono-phase liquid bearing, (2) mono-phase vapor bearing; (3) bi-phase liquid and vapor bearing, vapor dominated; (4) bi-phase liquid and vapor bearing, vapor dominated; and (5) tri-phase liquid, vapor, and solid bearing inclusions. The mono-phase inclusions are interpreted to reflect metastability (failure of nucleation of the vapor phase) and locally necking down. The mono-phase vapor inclusions and some of the liquid-dominated bi-phase inclusions are interpreted to represent the vapor phase and liquid phase of an immiscible fluid system. The vapor-dominated and some of the liquid-dominated bi-phase inclusions are interpreted as heterogeneous trapping of both vapor and liquid from the immiscible system. The solid-bearing tri-phase inclusions mostly represent heterogeneous trapping of solid particles together with the fluid phase(s). The inclusions of interest for further microthermometric and chemical analysis were the bi-phase, liquid dominated, aqueous inclusions of a primary or pseudosecondary origin. In total, ninety-four inclusions from ten fluid inclusion assemblages (FIA; Goldstein and Reynolds 1994) and fluid inclusion domains (areas populated by fluid inclusions close to each other that cannot be strictly treated as a FIA) were analyzed by means of microthermometry and Raman spectroscopy. During the heating phase of microthermometric experiments the inclusions homogenized to the liquid phase between 105°C and 130°C. During cooling, many of the inclusions showed reluctance to freezing, while those that did freeze required supercooling to -180°C. First melting temperatures were found to be in the range of -55°C to as low as -69°C. Ice melting was observed between -37°C and -23°C. When observed, hydrohalite melting took place between -50°C and -35°C, however this was not the general case. Hydrohalite melting was then assumed to be synchronous with ice melting when crystals of hydrohalite were too fine-grained to accurately observe melting. It is also possible that hydrohalite was not formed during cooling and therefore the melting of ice represents a metastable phenomenon. In many cases, Raman spectroscopic analyses indicated that halite rather than hydrohalite was the last phase to melt, which took place between -5°C and 8°C.

The observed first melting, ice melting, hydrohalite melting, and halite melting temperatures indicate that the fluid may be characterized by the H_2O-NaCl-$CaCl_2$ system, which was verified by means of cryogenic Raman spectroscopy. The fluid salinity was then estimated by inputting two of either ice, hydrohalite, or halite melting temperatures into the program of Steele-McInnis (2010). Fluid salinities calculated from these temperatures vary between 22 and 29 wt.% NaCl equivalent. These results are typical of an URU deposit in the Athabasca Basin and the range in fluid salinity overlaps with other studies from deposits in both the eastern Athabasca basin and the

western Patterson Lake Corridor. The range of homogenization temperatures (105 - 130°C), together with the interpretation of fluid immiscibility, indicate that the mineralization took place at a shallow depth (<3 km rather than > 6 km as assumed in previous studies), as proposed by Chi et al. (2018). On-going LA-ICP-MS analysis of fluid inclusions will provide more information about the fluid composition, especially trace elements. These will be used to evaluate further the mechanism of uranium mineralization and its relationship with Ni-Co-As mineralization.

REFERENCES

Chi, G., Li, Z., Chu, H., Bethune, K.M., Quirt, D.H., Ledru, P., Normand, C., Card, C., Bosman, S., Davis, W.J., Potter, E.G. (2018) A shallow-burial mineralization model for the unconformity-related uranium deposits in theAthabasca Basin. Economic Geology, v. 113, p. 1209-1217.

Goldstein, R.H., and Reynolds, T.J., 1994, Systematics of fluid inclusions in diagenetic minerals: Society for Sedimentary Geology (SEPM) Short Course, v. 31, p. 199.

Steele-MacInnis, M., Bodnar, R.J. and Naden, J. (2010) Numerical model to determine the composition of H_2O-NaCl $CaCl_2$ fluid inclusions based on microthermometric and microanalytical data. Geochimica et CosmochimicaActa, v. 75, p. 21-40.

A melt inclusion study of rhyolitic volcanics in the Bousquet Formation, Doyon-Bousquet-LaRonde mining camp, Abitibi Subprovince, Québec: Insight into Archean magmatic processes

Jacob J. HANLEY[1], Daniel MEAGHER[1], Kevin NEYEDLEY[1], Zoltán ZAJACZ[2], Alexandra TSAY[2], and Patrick MERCIER-LANGEVIN[5]

[1]*Department of Geology, Saint Mary's University, Halifax, Nova Scotia, Canada*

[2]*Department of Earth Sciences, University of Geneva, Geneva, Switzerland*

[3]*Natural Resources Canada, Geological Survey of Canada, Québec, Québec, Canada*

E-mail: jacob.hanley@smu.ca

Silicate melt inclusions (SMI) in rhyolitic volcanic rocks in the ~2699 – 2697 Ma Bousquet Formation, Doyon-Bousquet-LaRonde (DBL) mining camp, Abitibi Subprovince, Québec were studied through integration of a variety of microanalytical methods (petrography, laser Raman microspectroscopy, LA-ICP-MS) to explore links between magmatic metal/volatile endowment and the high Au content in some VMS deposits of the DBL camp (Mercier-Langevin et al., 2007). The study is the first to present trace element/ore metal data for SMI of this age globally.

Rhyolitic SMI of primary origin (Fig. 1) were characterized from magmatic quartz phenocrysts of quartz feldspar porphyry (QFP) tholeiitic rhyolite sills (Unit 2; lower Bousquet) and calc-alkaline flows (Unit 5.3; upper Bousquet) at the LaRonde-Penna and Westwood deposits. SMI trace element discrimination records a continuous transition from ocean ridge (ORG) to volcanic arc (VAG) tectonic affinity from the lower to upper Bousquet formations. SMI trace element (Sr-Y-La-Yb) characteristics are inconsistent with Archean tonalite-trondhjemite-granodiorite (TTG; "adakitic") compositional domains; rather, they are consistent with post-Archean TTG ("calc-alkaline") suggesting significant compositional modification of TTG magmas through contamination and/or plagioclase fractionation.

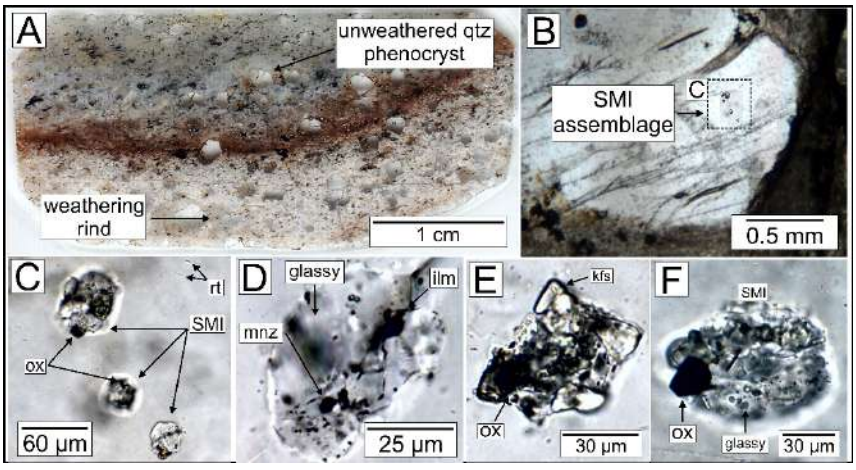

Figure 1. Representative photomicrographs of SMI hosted in quartz from units 2.0 and 5.3 of the Bousquet Formation. All images taken in transmitted PPL. (A) Thin section of partially weathered rhyolite from a unit 2.0 surface sample; SMI were analyzed from unweathered quartz phenocrysts. (B) SMI assemblage containing 3 inclusions; dashed area is enlarged in frame (C). (C) Partially recrystallized SMI assemblage [enlarged view from (B)]. (D) A partly recrystallized SMI containing monazite and ilmenite daughter phases. (E-F) Recrystallized SMIs containing oxide and feldspar daughter phases, possibly accidentally trapped. Note: kfs = feldspar, ilm = ilmenite, mnz = monazite, ox = oxide, qtz = quartz, rt = rutile, SMI = silicate melt inclusion.

SMI major and trace element data record significant differentiation of rhyolites (at least 70 %), and thermobarometry suggests prolonged phenocryst residence and SMI entrapment at ~10-12 km depth. Notably, SMI concentrations of Au (1st to 3rd quartile range: 6-160 ppb), Cu, As, Sn, Sb, Bi, and Pb are widely variable and up to two orders of magnitude higher than in the host bulk volcanic rocks (Fig. 2). This demonstrates that whole rock data are not representative of the composition of the original magmatic liquids and questions the validity of the traditional use of whole rock data as a proxy for volcanic assemblage fertility in such Archean environments. The SMI show melt co-entrapment with immiscible, high density, carbonic fluid (CO_2-dominant), indicating that rhyolitic melts were saturated in CO_2 (Fig.3).

Saturation of this fluid phase may explain, in part, the variability observed in SMI metal contents, and demands consideration of the relative importance of early separation of magmatic volatile phases versus seafloor hydrothermal leaching of volcanic products in controlling the Au and related magmatic metal endowment of Archean VMS ore-forming systems.

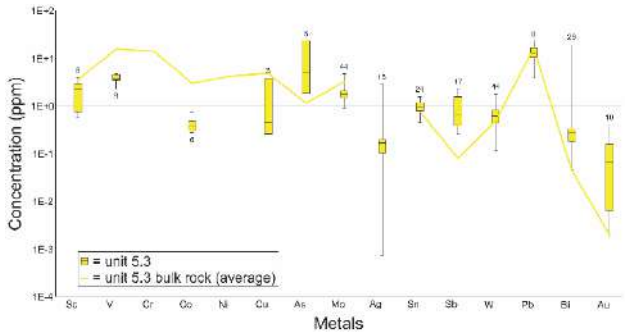

Figure 2. Box and whisker plot of metals from units 5.3 SMI. Shown are the 1st and 3rd quartile ranges, averages, and error bars of metals. Metal concentrations were collected by LA-ICP-MS. Numbers near each box and whisker represent the number of SMI with analyses above detection limit. Bulk rock data are averages from collected samples and overlay the box and whiskers for comparison.

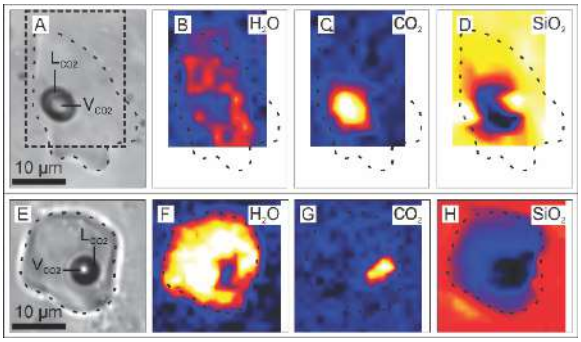

Figure 3. Raman maps of a homogenized SMI from unit 5.3. The mapped areas for H_2O, CO_2, SiO_2 are based on intensity ranges 3450-3650 cm^{-1}, 1385- 1390 cm^{-1}, and 450-475 cm^{-1}, respectively. (A) PPL image of a homogenized SMI with a large liquid and vapour CO_2 bubble in glass. (B-D) Intensity distribution of H_2O, CO_2, and SiO_2 in the homogenized SMI and surrounding host quartz. (E) PPL image of a homogenized SMI with a large liquid and vapour CO2 bubble in glass. (F-H) Intensity distribution of H_2O, CO_2, and SiO_2 in the homogenized SMI and surrounding

REFERENCES

Mercier-Langevin, P., Dubé, B., Lafrance, B., Hannington, M., Galley, A., Moorhead, J., and Gosselin, P. (2007). Metallogeny of the Doyon-Bousquet-LaRonde mining camp, Abitibi greenstone belt, Quebec, *in* Goodfellow, W.D., ed., Mineral deposits of Canada: A synthesis of major deposit-types, district metallogeny, the evolution of geological provinces, and exploration methods: Mineral Deposits Division, Geological Association of Canada, Special Publication no. 5, p. 673–701.

Fluid chemistry of the Archean Chibougamau porphyry-type Cu(-Au) system: An aqueous-carbonic magmatic hydrothermal ore system

Daniel J. KONTAK[1], Lucy MATHIEU[2], Alexandre CRÉPON[2]

[1]*Harquail School of Earth Sciences, Laurentian University, Sudbury, Ontario, Canada;*

[2]*Université du Québec à Chicoutimi (UQAC), Chicoutimi, Québec, Canada;*

E-mail: dontak@laurentian.ca

Porphyry-type mineralized ore deposits (PCDs; Cu, Mo, Au, PGEs) are abundant in the Phanerozoic rock and have been extensively studied. They represent the end product of solidified, volatile-saturated upper crustal magmas. Expulsion of the latter fluids from intermediate to felsic magmas into an extensively fractured carapace forms a series of planar and stockwork veins (e.g., EDM, A-D types) associated with a series of zonal arranged alteration types (i.e., potassic, phyllic, argillic, propylitic). These aforementioned features are generally considered to be diagnostic of PCDs. Similarly, extensive studies of vein fluids in numerous PCDs preserved as fluid inclusions (FIs) indicate three dominant aqueous fluid types (e.g., Bodnar et al., 2014): 1) intermediate density of low-salinity (i.e., <5-10 wt. % eq. NaCl); 2) low-density V-rich; and 3) high-density, hypersaline (i.e., >40 wt. % eq. NaCl). Whereas type 1 is the primary fluid, types 2 and 3 are a complementary pair formed from unmixing of type 1. Although the presence of a carbonic component is noted in FIs from PCDs, it is uncommon. In contrast to their abundance in the Phanerozoic record, PCDs are rare in the Precambrian and even more so for the Archean. Due to the latter, the fluid chemistry of older putative PCD systems are poorly studied, which is important in regards to contrasting them with younger analogues. Here we report results of a FI study of a well-known Archean intrusion-hosted Cu-Au vein setting in Chibougamau, Quebec, known as the Central Camp (see Mathieu and Racicot (2019) for summary).

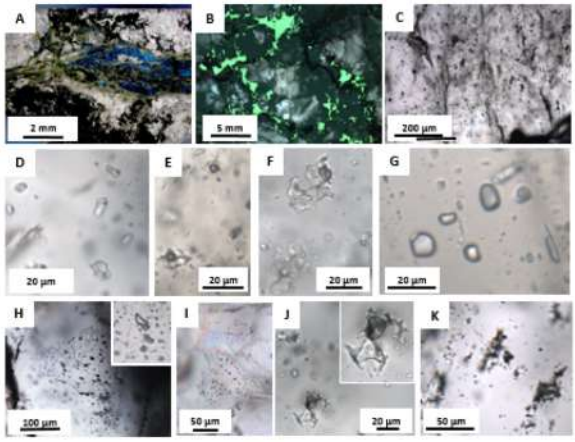

Figure 1. A, B) Veins with Biotite-Chlorite alteration (A) and Cpy (B); C) typical FIAs in quartz; D, E) Type 1 FIs; F) Type 2 FIs; G-I); J) Type 4 FIs; K) Type 5 FIs.

The Neoarchean Chibougamau pluton, located in the NE part of the Au-endowed Abitibi greenstone belt (AG) of the Superior Craton, is a polyphase composite body of ca. 2617 Ma emplaced at the terminal stage of the main construction phase of the host greenstone rocks. It is dominated by diorite-tonalite with small volume quartz-feldspar porphyry dikes (trondhjemite?), thus a TTD suite. In the Central Camp, inter-mineral dikes indicate that the main mineralizing phase is coeval with the 2718-2716 Ma intrusive phase. Structurally controlled, Chibougamau-type mineralization is divided into vein versus breccia styles with the former having two sub-types, sulfide versus magnetite dominant. The sulfide-type zone, the focus of this study, consists of disseminated- to massive pyrite, chalcopyrite (cpy) and pyrrhotite with some sphalerite-galena micro-inclusions; gangue minerals are chlorite, carbonates, quartz, and sericite. This mineralization appears as stockworks, veins subparallel to foliation, or as late carbonate-quartz-cpy veins. Magnetite-type zones, now localized to shear zoned, are locally seen to cut Chibougamau-type sulfide zones. These massive massive-magnetite bodies ± carbonate ± pyrite are but by laminated quartz-carbonate-tourmaline-pyrite-cpy-pyrrhotite veins with rare visible gold and rare sphalerite-galena.

The cpy-bearing samples studied show cpy occurs (Fig. 1A, B): 1) coating fractures that traverse quartz; 2) surrounding euhedral or anhedral (i.e., dissolved) quartz; or 3) intergrown with green, Fe-rich biotite that is retrograded to chlorite. FIs in well preserved (i.e., not strained) quartz was studied from several samples with two exceptional samples of quartz-carbonate-pyrite-cpy veins used for microthermometry. In all samples studied (n=10), fluid inclusion assemblages (FIA) corresponding to discrete fluid trapping events were identified (Fig. 1C) (i.e., primary (P), secondary (S), pseudosecondary (PS), indeterminate (I)) and are described below along with

preliminary results of microthermometry for two of these. **Type 1 FI (L_{H2O}-V_{H2O})** occur as I, S, and PS with variable L:V ratios used to subdivide them with type 1a (<10-15% V; Fig. 1D)) and type 1b (>15% V; Fig. 1E). Large ranges in Th are noted for type 1a (85 to 145°C) and 1b (205 to 400°C; some decrepitated at 340°C). Both types are highly saline (24 to 31 wt. % eq. NaCl) and Ca-rich ($CaCl_2$/NaCl = 6 to 15 based on ice-hydrohalite melting). **Type-2 FI** (L_{H2O}-V_{H2O}-Halite±Solids) are common and generally contain <10-15% V and variable % solids (Fig. 1F) which is attributed to necking. They occur as I, S, and PS types and have Th(Tot) between 170 to 400°C with salinities of 29 to 50 wt. % eq. NaCl. Multi-solid FIs with irregular shapes (including decrepitates) show no detectable phase change when heated to 450°C. **Type-3 FI** (V_{H2O}-rich) have >90% V (Fig. 1G) and variably occur as P, S, PS, and I types coring quartz grains (Fig. 1H), decorating grain surfaces (Fig. 1I), defining subparallel elongate planes, on ductile micro-fractures, and along grain boundaries. Cooing to 196°C did not reveal phase changes, hence these FIs are considered V_{H2O} versus mixed COHN types; for one FIA Fig. 1G) narrow liquid rims indicate salinities of 9 wt. % eq. NaCl. **Type 4 FI** are two (L_{H2O}-V_{CO2}) and three (L_{H2O}-L_{CO2}-V_{CO2}) phase aqueous-carbonic types at room temperature that occur as isolated clusters, thus I types. They are most common as irregular-shaped decrepitates with neonate haloes (Fig. 1J) versus equant shapes (Fig. 1K). Limited microthermometry (2 FIAs) indicate Tm(CO_2) of -57°C, Tm(clath) of +5°C, and Th(CO_2) of 26-28°C. **Type 5 FI** denote FIs with decrepitate textures (Fig. 1K), which includes types 1 and 4; these FIs are abundant. The chemistry of FI was quantified using evaporate mounds that were imaged and analyzed with an SEM-EDS system. Results indicated a multi-component fluid chemistry dominated by Na-Ca (±Fe, K, Mn, Ba) and Cl (±S, F) (Fig. 2).

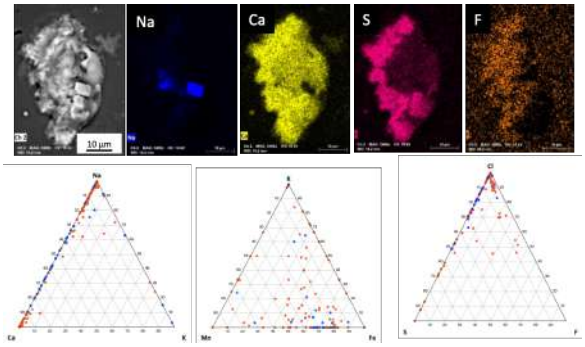

Figure 2. Top: Mound image from SEM with equivalent X-ray maps. Bottom: Ternary plots (wt. %) for point (red) and raster (blue) mound analyses.

Results of this preliminary study of FIs in an Archean Cu(-Au) PCD setting highlight several important features: 1) the FIAs noted contrast markedly with orogenic gold fluids (Bodnar et al. 2014), in particular those of the AGB (Tuba et al., 2021); 2) the FIAs compare with some PCDs where aqueous-carbonic fluids are noted (Mao et al. 2017); 3) FI chemistry is more consistent with magmatic-hydrothermal (e.g., PCDs; Bodnar et al. 2014) versus metamorphic fluids; and 4) abundant decrepitated FIs (type 5) suggest Pcycling, a feature for PCDs (e.g., Tsuruoka et al. 2019). Additionally, the FIAs and fluid chemistry for the Chibougamau setting are comparable to that for the 2740 Ma Côté Gold porphyry-type Au(-Cu; +10 Moz Au) deposit of the Superior Province (Gourcerol et al. 2017).

REFERENCES

Bodnar, R.J. et al. (2014) Fluid inclusions in hydrothermal ore deposits, Treatise on Geochemistry, Second Edition 13, 119-142. Oxford: Elsevier.

Gourcerol, B. et al. (2017) Reconstruction of the PTX conditions of an Archean porphyry-type deposit: the 2740 Ma Cote Gold Au(-Cu) deposit, Canada. ECROFI Meeting, Nancy, France, Abstract Vol.

Kontak, D.J. and Tuba, G. (2017) How can fluid inclusion studies better constrain orogenic gold deposit models?: Case studies from the Superior Province and Meguma Terrane, SGA Meeting, Quebec, Canada, Abstract Vol.

Mao, W. et al. (2017) Physical and chemical evolution of the Dabaoshan porphyry Mo deposit, South China: Insights from fluid inclusions, CL, and trace elements in quartz, Economic Geology, 112, 889-918.

Mathieu, L. and Racicot, D. (2019) Petrogenetic study of the multiphase Chibougamau pluton: Archaean magmas associated with Cu-Au magmato-hydrothermal systems, Minerals, v. 9: 174, doi:10.3390/min9030174.

Tsuruoka et al. (2019) Evolution of the magmatic-hydrothermal system at Santa Rita porphyry Cu Deposit, New Mexico, USA: Importance of intermediate-density fluids in ore formation. Economic Geology, 116, 1267-1284.

Tuba, G. et al. (2021) Fluid diversity in the gold-endowed Archean orogenic systems of the Abitibi greenstone belt (Canada) I. Constraining the PTX of prolonged hydrothermal systems. Ore Geology Reviews, v. 135, doi.org/10.1016/j.oregeorev.2021.104221

Fluid Inclusion Analysis of Halite from the Early Cambrian Ouldburra Formation, Eastern Officer Basin, Australia: A Snapshot of the Cambrian Explosion

Amy LEFEBVRE[1], A. MORRISON[1], N.J.F. BLAMEY[1], U. BRAND[2]
[1]*Dept. Earth Sciences, University of Western Ontario, London;*
[2]*Dept. Earth Sciences, Brock University, St Catharines.*
E-mail: alefebv8@uwo.ca

Halite grows at the interface between atmosphere and brine, and in so doing, offers a unique opportunity to sample ancient atmospheric gases and fluids. The fluid inclusions are trapped at ambient conditions and at standard atmospheric pressure, therefore the trapping temperatures reflect the actual conditions without the need for isochors and pressure corrections. Another advantage of halite-hosted fluid inclusions forming at the contact between brine and atmosphere is that bubbles of atmospheric gases become trapped, affording the opportunity to analyze fossil gases and sample the Earth's atmosphere through geological time.

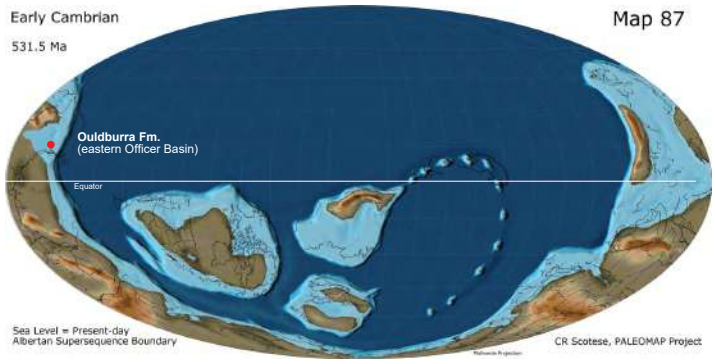

Figure 1. Locality diagram of the Ouldburra Formation of the Eastern Officer Basin during the Early Cambrian (modified from Scotese, 2014).

In this study, halite from the early Cambrian Ouldburra Formation (Eastern Officer Basin) of Australia was examined for their geochemistry and microthermometry (Fig. 1). The samples were acquired from drill core housed at the Southern Australia Core Library in 2019, specifically from the Manya-6 core. This core was previously studied and the halite is reported in Kovalevych et al. (2006). Samples were examined in hand specimen for preservation, following the screening protocol presented by Blamey and Brand (2019). Halite varies in colour from red or tannish to white or clear. Most commonly, bedded halite is clear to tannish, and is bounded by sediment of several mm thickness. In contrast, the reddish halite is invariably discrete crystals that are hosted within sediment. Core with primary growth features were targeted for sampling (Fig. 2).

Figure 2. Primary red halite from the Manya-6 core.

Only primary fluid inclusions were examined in this study. The methods applied include petrography, microthermometry, fluid inclusion gas analysis by mass spectrometry, trace element analysis of the halite mineral. Using petrography, the primary fluid inclusions are recognized by their square shape, as well as by their tendency to form Fluid Inclusion trails (FIT) that are orientated along the crystallographic axes of halite. At room temperature, the fluid inclusion bubbles are generally either very small or absent, which reflects the ambient temperatures at which halite precipitates. Microthermometry was conducted using a Linkham stage, the calibration confirmed daily using a pure water standard. Fluid inclusion gas analysis was performed on about 150 mg of halite, and crushed incrementally to produce 8-10 crush-results per sample.

The microthermometry results of the samples range from 15 to 45 degrees Celsius (Fig. 3). At the deepest and oldest area of the halite sample, the temperature ranges from 20 to 40 degrees Celsius. These temperature ranges are consistent throughout the middle of the halite sample. As the length of the sample increases, the younger

rock samples temperatures decrease slightly, ranging from 20 to 30 degrees Celsius, + or - 5. At the uppermost area of the halite, temperatures are highest, ranging from 35 to 45 degrees Celsius. Moreover, the fluid inclusion gas analysis results were more variable than expected, however, the best samples gave atmospheric oxygen levels in the 15 to 20 percent pO_2.

The trends observed by the results described above correspond to the theorized rising hot-house conditions of the Cambrian period. Notably, the temperature of the rock continually increases throughout its formation, providing evidence to support this environmental change. The oxygen levels of 15-20% pO_2 obtained using the gas analysis method are lower than Earth's current oxygen levels, but higher than the ~11% pO_2 reported by Blamey et al. (2016) for the Neoproterozoic period. Notably, these findings match the atmospheric oxygen values reported in Brand et al. (2021) for the end of the Ediacaran.

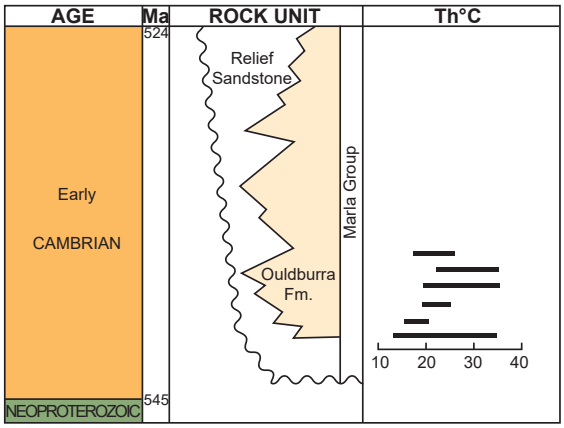

Figure 3. Temperature trends based on micro thermometry of the Ouldburra Formation during the Early Cambrian (modified from Kovalevych et al., 2006).

Throughout the analysis of the Ouldburra halite samples, the temperature trends within the fluid inclusions, as well as oxygen and bromine content of these samples, were established. The microthermometry results presented a rising temperature trend, matching the hypothesised greenhouse temperature of this time-period. Gas analysis has determined that the atmospheric oxygen ranges between 15-20% pO_2, which is lower than current oxygen levels for Earth's atmosphere. Br content has narrowed the range of this element within the halite samples, confirming that the present-day intracontinental location, matches its location at the time of its formation. Overall, these findings provide substantial support of the rising hot-house conditions during the Cambrian period and concomitant biological explosion.

REFERENCES

Blamey, N.J.F., and Brand, U. (2019) Atmospheric gas in modern and ancient halite fluid inclusions: A screening protocol, Gond. Res. 69, 163-176.

Blamey, N.J.F., et al. (2016) Paradigm shift in determining Neoproterozoic atmospheric oxygen, Geology 44, 651-654.

Brand, U., et al. (2021) Atmospheric oxygen of the Paleozoic, Ear.-Sci. Rev. 216, 103560.

Kovalevych, V.M., et al. (2006) Deposition and chemical composition of Early Cambrian salt in the eastern Officer Basin, South Australia, Aust. J. Ear. Sci. 53, 577-593.

Scotese, C. R. (2014) Atlas of Silurian and Middle-Late Ordovician Paleogeographic Maps (Mollweide Projection), Maps 73-80, Volumes 5, The Early Paleozoic, PALEOMAP Atlas for ArcGIS, PALEOMAP Project, Evanston, IL., *1*.

Fluid modeling and U-Pb dating constraints on fluid evolution history in 1D basin modeling framework

Xiuyan LIU[1, 2], Jacques PIRONON[1], Alexy ELIAS BAHNAN[1]
[1]*Université de Lorraine, CNRS, GeoRessources lab, 54000 Nancy, France*
[2]*China University of Geosciences, Wuhan 430074, China*
E-mail: xiuyan.liu@univ-lorraine.fr

Fluid inclusions and 1D basin modeling techniques are commonly used to investigate fluid evolution histories in sedimentary basins. Trapping temperatures of fluid inclusions can be compared relative the burial temperatures to assess the relative timing of fluid circulation. Absolute age dating of minerals can give additional age constraints on fluid and basin modeling results. To this end, fluid inclusions from the Lower Cambrian Niutitang shales from the Danquan outcrop, SE Chongqing, China, were studied to understand the fluids and formation P-T evolution histories.

The study area was a passive continental margin and underwent rapid subsidence during the Cambrian to Silurian. A depositional hiatus is recorded between the Devonian to early Permian, followed by rapid subsidence from Triassic to middle Jurassic (170 Ma). Then, uplifting began and caused an erosion of around 6 km during the middle Jurassic (170 Ma) to present-day. The present-day study area is folded into a series of Jurassic anticlines and synclines. Samples were collected from an anticline in the Danquan area for petrographic and fluid inclusion analyses.

After constructing a paragenetic sequence involving apatite, calcite 1, dolomite, quartz, and calcite 2, microthermometry was done on the FI-rich calcite 1, quartz and calcite 2. In each mineral, the FIs were classified into clusters, isolated and trails. All the clusters and isolated FIs are within single mineral crystals, possibly indicating a primary origin. The trails in calcites and quartz end within single crystals, indicating a pseudosecondary origin. The T_h of primary and pseudosecondary FIs in calcite 1 shows one mode of 120 °C. The T_h of primary and pseudosecondary FIs in quartz shows one mode of 140 °C. The T_h of primary and pseudosecondary FIs in calcite 2 shows one mode at 140 °C.

Raman spectroscopy analysis was done to determine the salinities (wt.% NaCl) (Caumon et al., 2013) and gas contents (Caumon et al., 2014) of the aqueous FIs. The results show that all studied FIs have salinities between 0 to 4.5 wt.% NaCl. No difference was seen between FIs of different origins or in different mineral phases. Out of 40 measurements, one methane-bearing aqueous FI was identified in calcite 1 having a methane content of 0.254 mol/kg H_2O, and four methane-bearing aqueous FIs in quartz with the methane content varying from 0.071 to 0.197 mol/kg H_2O.

U-Pb isotope dating (Chew et al., 2014) was carried out on apatite, dolomite, and calcite 2. The U/Pb age of apatite is 544.12±5.66 Ma, while the dolomites have an age of 318.2±81.3 Ma, and the calcite 2 yields an age of 3.43±1.54 Ma. These three ages lay additional constrains on the paragenesis.

To determine the trapping temperatures of primary inclusions, the equation of state (EoS) of Duan and Mao (2006) was used to calculate their homogenization pressure (P_h). The EoS of Zhang and Frantz (1987) was used to draw the isochores of the aqueous FIs without gas contents. The double-isochore method was not possible in this case because no pure hydrocarbon inclusions were detected. Instead, the intersection of the isochores with the hydrostatic and lithostatic gradients, calculated from Petromod 1D, was used as the minimum and maximum P-T conditions of fluid entrapment. The heat flow in Petromod 1D was modified reversely to let the modeled ages of calcite 1 at minimum and maximum P-T conditions be between the U-Pb ages of apatite and dolomite, and the modeled ages of quartz be younger than the U-Pb age of dolomite.

The preliminary results show that, at hydrostatic condition, the calcite 1 precipitated at around 430 Ma at a temperature of 140 °C, whereas at lithostatic condition, the calcite 1 precipitated at around 258 Ma at 178 °C. The quartz precipitated at 271 Ma at a temperature of 165 °C at hydrostatic condition, and it precipitated at 250 Ma at 205 °C at lithostatic condition. The calcite 2 precipitated at 132 Ma with a temperature of 167 °C under hydrostatic condition during the uplifting, whereas it would precipitate at 157 Ma at 217 °C if the lithostatic

condition was reached. The FIs in quartz, reach the highest temperature of around 250 °C, suggesting the formation was heated to at least 250 °C at the maximum burial.

Note that the ages (132-157 Ma) of calcite 2 determined from fluid and basin modeling is different from its U-Pb age (3.43±1.54 Ma), and the formation temperature calculated by Petromod 1D is around 27 °C at 4 Ma, which is much lower than the T_h mode (140 °C) of primary and pseudosecondary FIs in calcite 2. There are several possible reasons that may cause such large differences. 1) The calcite 2 precipitated from a pulse of hydrothermal fluids at around 4 Ma, which was in disequilibrium with the host rock. 2) The U-Pb age of calcite 2 was affected by secondary alterations during the uplifting, such as leaching of fluids that caused a lead loss. And 3) The calcite 2 experienced partial recrystallization at 4 to 3 Ma and was partially preserved. However, there is no regional geological events that can be related to the possible hydrothermal event at around 4 to 3 Ma. Besides, if the lead loss had happened, the points with high U-Pb ratio would be highly dispersive on the Tera-Wasserburg diagram, but not arrange in a line like in our results suggesting our U-Pb age is reliable. Therefore, the most likely reason is the calcite precipitated at sometime between 157 to 132 Ma, but partially recrystallized at 4 to 3 Ma. Some of our U-Pb points were on the recrystallized calcite 2, and therefore, yielded a very young U-Pb age.

Our study shows that fluid modeling and absolute age determination of host minerals can give additional constraints on the fluids and formation P-T evolution histories in areas with complex geodynamic backgrounds.

REFERENCES

Caumon, M.-C. et al. (2013) Fused-silica capillary capsules (FSCCs) as reference synthetic aqueous fluid inclusions to determine chlorinity by Raman spectroscopy, Eur. J. Mineral. 25, 755-763.

Caumon, M.-C. et al. (2014) Determination of methane content in NaCl–H2O fluid inclusions by Raman spectroscopy. Calibration and application to the external part of the Central Alps (Switzerland), Chem. Geol. 378, 52-61

Chew, D.M. et al. (2014) U–Pb LA–ICPMS dating using accessory mineral standards with variable common Pb, Chem. Geol. 363, 185-199.

Duan, Z., Mao, S. (2006) A thermodynamic model for calculating methane solubility, density and gas phase composition of methane-bearing aqueous fluids from 273 to 523 K and from 1 to 2000 bar, Geochim. Cosmochim. Acta 70, 3369-3386.

Zhang, Y.-G., Frantz, J.D. (1987) Determination of the homogenization temperatures and densities of supercritical fluids in the system NaClKClCaCl2H2O using synthetic fluid inclusions, Chem. Geol. 64, 335-350.

The End Ordovician Icehouse and the First Mass Extinction of the Phanerozoic: Its History Recorded in Halite

Audrey K. MORRISON[1], Amy LEFEBVRE[1], Ariel V. PATTER[1], Alyssa M. DAVIS[2], Uwe BRAND[2], Nigel J.F. BLAMEY[1], Jisuo JIN[1].

[1]*Department of Earth Sciences, University of Western Ontario*
[2]*Department of Earth Sciences, Brock University*
E-mail: amorr224@uwo.ca

During the latest Ordovician (Hirnantian Age, ~443–442 Ma) a double-pulsed Mass Extinction event wiped out an estimated 60% – 85% marine organisms at the generic taxonomic level (Alroy et al., 2008; Fan et al., 2022). Although the cause of the extinction is highly debated, new data suggest that sudden, abrupt, and extensive glaciation was to blame. Analysis of halite samples from two separate locales of similar latitude during the Late Ordovician-Earliest Silurian suggest that severe temperature fluctuations emulate a transition into an icehouse phase. Though the Hirnantian Stage is suspected to only have lasted 0.47 ± 0.34 Ma (Ling et al., 2019), other evidence of multiple cooling pulses suggests the event may have lasted into the Earliest Silurian. Primary fluid inclusions of the mineral halite were analyzed to reveal formation temperatures. Its cubic structure allows for upward-growing chevrons to develop at the bottom of brine pools. During this process, cavities within the crystal fill with brine, trapping and preserving fluid as it is not affected by recrystallization or dissolution (Handford, 1991). Cavities of this nature are primary fluid inclusions. In contrast, secondary fluid inclusions were avoided in our analysis as brine in those cavities have undergone alteration and are not indicative of the mineral's initial environment.

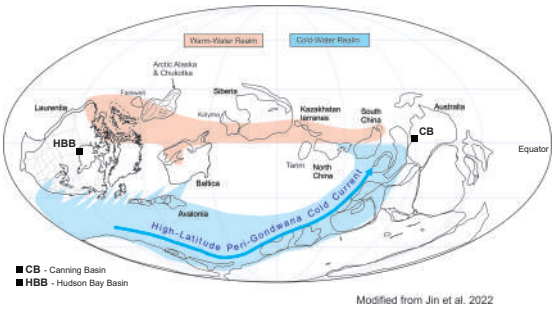

Figure 3: Locality diagram of the Hudson Bay Basin (Red Head Rapids Fm.) and Canning Basin (Mallowa Salt) the during the Hirnantian Stage.

Halite samples were obtained from two localities. During the Hirnantian both were near the equator, but half a world apart (Figure 1). The first location represents mid-Upper Ordovician and Silurian strata of the Hudson Bay Basin during the End Ordovician (Zhang, 2010). The halite was obtained from the Red Head Rapids Formation, which is an evaporite-dominated succession within the region (Lavoie et al., 2013). The samples are from the top of the Red Head Rapids Formation of the Aquitaine Sogepet et al. Pen No. 1 Core. Its depth ranges between 792 and 795 meters representing a total of 5 samples. The second location comprises of the Carribuddy Group of the Canning Basin of central northern Western Australia. The Carribuddy Group has been subdivided into the following five formations, in ascending order, the: Bongabinni, Minjoo Salt, Nibil, Mallowa Salt, and Sahara (Haines, 2009). The selected halite interval consisted of 10 samples from the Mallowa Salt of the Brooke-1 (BHP-Utah) Core. Its depth ranges between 1172.55 meters and 1417.20 meters. It should be noted that controlled tectonic uplift, subsidence and eustatic alteration aided in the evolution of each locale, while the primary halite fluid inclusions remained unchanged. When analyzing temperature data, calculated average temperatures per sample are insufficient in depicting temperature trends. Averaging the range of temperatures disregards any oscillations (daily, seasonal, annual) that could be characteristic of cooling/warming pulses. In this study temperatures were divided into 8 bins. Bins 14°C-17°C, 17°C-20°C, 20°C-23°C, and 23°C-26°C represent lower temperatures while bins 26°C-29°C, 29°C-32°C, 32°C-35°C,

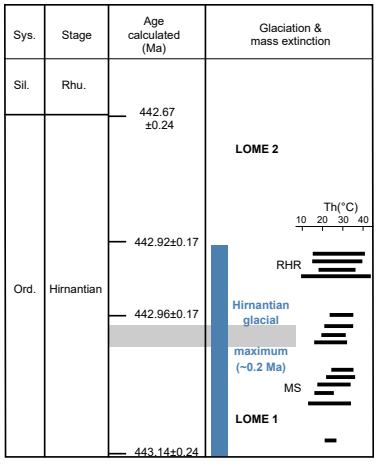

Figure 4: Temperature trends based on micro thermometry of the Red Head Rapids Formation (RHR) and Mallowa Salt (MS) during the Hirnantian Stage of the End Ordovician (Ord.) and Late-Ordovician Mass Extinctions (LOME) (modified from Ling et al., 2019).

and 35°C-38°C represent higher temperatures. A temperature of 26.5°C was the boundary between high and low temperatures, with each individual reading being rounded to the nearest degree. Microthermometry of ten samples from the Mallowa Salt Members showed three cooling periods in the sequence. The daily temperature fluctuations depict a bimodal trend apart from three samples. Samples at depths between 1194.14-1194.24 meters, 1263.5-1263.55 m and 1417.10-1417.20 m from the Brooke-1 core showcase significant cooling trends as the majority of temperatures plot within the low temperature bins. These three low temperature pulses probably correspond to pulses within the glaciation event noted during the early Ordovician. Microthermometry of the Red Head Rapids Formation halite exhibit a similar bimodal trend. Four of the five samples display daily temperature fluctuations more extreme than that of the Mallowa Salt. Thus, an additional low temperature bin of 11°C -14°C was added. Temperatures as low as 10°C were recorded within the four samples hosting primary fluid inclusions. These temperatures are especially significant due to Hudson Bay Basin's location near the paleoequator. In a tropical environment, there should be no significant variation between its wet and dry seasons. Average temperatures from the Red Head Rapids ranged between 22°C and 24°C, characteristic of daily variation. For the two locations, the average temperature estimated for the End-Ordovician-Earliest-Silurian is 24.2°C ± 0.5°C. A comprehensive reassessment of previous ocean temperature data of the Phanerozoic by Grossman & Joachimski (2022) compared paleotemperature projections between four major studies. The paleotemperatures varied greatly during the End-Ordovician Earliest-Silurian boundary interval. Three publications (Grossman & Joachimski, 2022, Song et al., 2019, and Veizer et al., 2020) showcased estimated average temperatures nearing 10°C or 35°C using oxygen isotope-determined temperatures on a variety of carbonates and/or phosphates. However, these extremes could be characteristic of variation within seawater -^{18}O values or sample alteration. Scotese et al. (2021) produced temperature trends similar to those documented in this study. They used isotopic data and paleotemperatures based on paleo-Köppen climate belts to produce an average temperature of around 25°C. Between our two studies, using two different methods of temperature determination, they yielded similar results. This provides solid support for a multiple-pulsed glaciation event during the lower Hirnantian of the End-Ordovician.

ACKNOWLEDGEMENTS

We thank M. Lozon (Brock University) for drafting the figures. We also thank NSERC for financial support to AKM, UB, and JJ and UWO to NJB.

REFERENCES

Alroy, J., et al. (2008), Phanerozoic trends in the global diversity of marine invertebrates. *Science*, *321*(5885), 97–100.

Fan, J. X., et al. (2020), A high-resolution summary of Cambrian to early Triassic marine invertebrate biodiversity. *Science*, *367*(6475), 272–277.

Grossman, E.L., Joachimski, M.M. (2022), Ocean temperatures through the Phanerozoic reassessed. *Sci Rep,* 12, 8938.

Haines, PW. (2009), The Carribuddy Group and Worral Formation, Canning Basin, Western Australia: stratigraphy, sedimentology, and petroleum potential. *Geological Survey of Western Australia*, Report 105, 60p.

Handford, C. R. (1991), Marginal marine halite; sabkhas and salinas. *Developments In Sedimentology*, *50* 1-66.

Jin, J., et al. (2022), Warm-water *Tcherskidium* fauna (Brachiopodia) in the Lake Ordovician Northern Hemisphere of Laurentia and peri-Laurentia. *Journal of Paleontology*, 0(0), 1-18.

Ling, M.-X., et al. (2019), An extremely brief end Ordovician mass extinction linked to abrupt onset of glaciation. *Solid Earth Sciences*, *4*(4), 190–198.

Lavoie, D., et al. (2013), Geological framework, basin evolution, hydrocarbon system data and conceptual hydrocarbon plays for the Hudson Bay and Foxe Basins, Canadian Arctic. *Geological Survey of Canada*, Open File 7363, 210 p.

Scotese, C.R., et al. (2021), Phanerozoic paleotemperatures: The earth's changing climate during the last 540 million years. *Earth-Sci. Rev.* 215, 103503.

Zhang, S. (2010), Upper Ordovician Stratigraphy and Oil Shales on Southampton Island Field Trip Guidebook. Open File 6668, 42p.

FLUID INCLUSION TECHNIQUE FOR BASIN MODELING- A CASE STUDY

V. Nandakumar[1], Shivapriya S[2], Silpa Thankan[3]

[1,2,3]*National Facility for Geofluids Research and Raman Analysis, National Centre for Earth Science Studies, Ministry of Earth Sciences, Government of India, Thiruvananthapuram 695011, Kerala, India.*
E-mail: v.nandakumar66@gmail.com

The Temperature of homogenization (T_h) data of fluid inclusions obtained from microthermometric study are widely used for the thermal history modeling using software like PetroMod. Bottom Hole Temperatures (BHT) are widely used in oil industry for thermal calibration purposes. Compared to commonly used thermal calibration parameters such as Vitrinite Reflectance (VR_o),Bottom Hole Temperatures (BHT) and Heat flow measurements, fluid inclusion data obtained can help to constrain the temperature at the time of fluid entrapment in the geological past (Bodnar, 1990: Burruss, 1981; Goldstein, 2001). This paleo-temperature (T_h data obtained) estimated from fluid-inclusion study provides extra support to build the thermal models for PSM. Fluid inclusion data along with Rock-Eval pyrolysis analysis can help to predict the maturity of oil in terms of API gravity as well as the maturity of source rocks respectively. Hence, fluid inclusion study along with Rock-Eval analysis can play an important role in oil exploration.

Two exploratory wells RV-1 (Mumbai offshore basin) and KK4C-A1 (Kerala Konkan offshore basin), India were examined as part of this study. Microthermometric analysis helps us to find the temperature of homogenization (T_h) of coeval aqueous inclusions along with the hydrocarbon fluid inclusions (HCFIs) that helped to calibrate the PetroMod software. Here, the temperature of homogenization (T_h) falls in the range between 60-150°C indicating oil-window. API gravity obtained from HCFIs samples of RV-1 well is indicating light oil and KK4C-A1 well indicating heavy oil (Nandakumar and Jayanthi, 2016). The secondary data of Rock-Eval pyrolysis analyses were used to determine the source rock maturity of two wells. Source rock parameters such as S1, S2, and T_{max}, were used for calculating Hydrogen Index (HI), Oxygen Index (OI), Production Index (PI) etc. show that source rocks of RV1 well of Mumbai offshore are mature and that of KK4C-A1 well are immature. Total Organic Carbon (TOC) content present in different depths of RV-1 well is indicating desirable organic matter content (maximum TOC of 39 wt. % in the Paleoecene-Eocene sediments of Panna formation (2365–2385 m). On the other hand, TOC of organic matter present in the source rocks of Kasaragod formation (stratigraphic equivalent of Panna formation) in the KK4C-A1 well shows a maximum TOC of 2.33 wt. % only (3550–3555 m), indicating that the Palaeocene-Eocene sediments of Kasaragod formation is having poor source rock characteristics, due to which the generation of hydrocarbon might not have occurred.

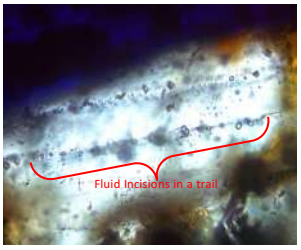

Figure 1. Fluid inclusion trails from the study area (Mumbai offshore basin, Western offshore, India).

Data generated using Fluid inclusion Technique (FIT) can be used in combination with the Petroleum System Modeling (PSM) software for understanding the generation and expulsion of oil in exploratory wells. PetroMod software (Version 2018.2) is an essential tool in oil exploration industry, and it contributes to the understanding of oil generation, expulsion, migration and to visualize the evolution of sedimentary basins (Nandakumar and Jayanthi, 2021). For basin modeling some preliminary data like age, thickness, lithology, Bottom Hole Temperature (BHT), seismic data and geochemical analysis etc. are essential. For better and more accurate results fluid inclusion microthermometric data were used in combination with PSM. For this study two sets of Petroleum System Models are created for the dry wells RV-1 and KK4C-A1 and calibrated each well using FIT and BHT to find the generation and expulsion. The Mumbai offshore well (RV-1) is showing ~1.2Mtons of maximum generation started from Early Eocene(~51Ma) to Pliocene and zero expulsion in BHT calibration model, whereas in FIT calibration model is showing a ~2.8Mtons of generation started from Early Eocene (~51Ma) to Pliocene and expulsion of ~2.4Mtons in Middle to Late Miocene (~10.1Ma) indicating an improved generation expulsion history. The dry well from Kerala-Konkan basin is showing a ~0.2Mtons of generation (~32Ma, Early Oligocene) and zero expulsion for BHT calibration model and FIT calibration model. Mackenzie heat flow calibration using BHT is done in most of the oil exploration industry, but our new approach for the calibration using the paleotemperature (T_h) from FIT is showing perfect fit into the curve

suggesting that FIT is a reliable method. Hence, the advantage of using FIT in PSM is highlighted in giving more robust output in terms of generation and expulsion than calibrating with other parameters like BHT and for PSM.

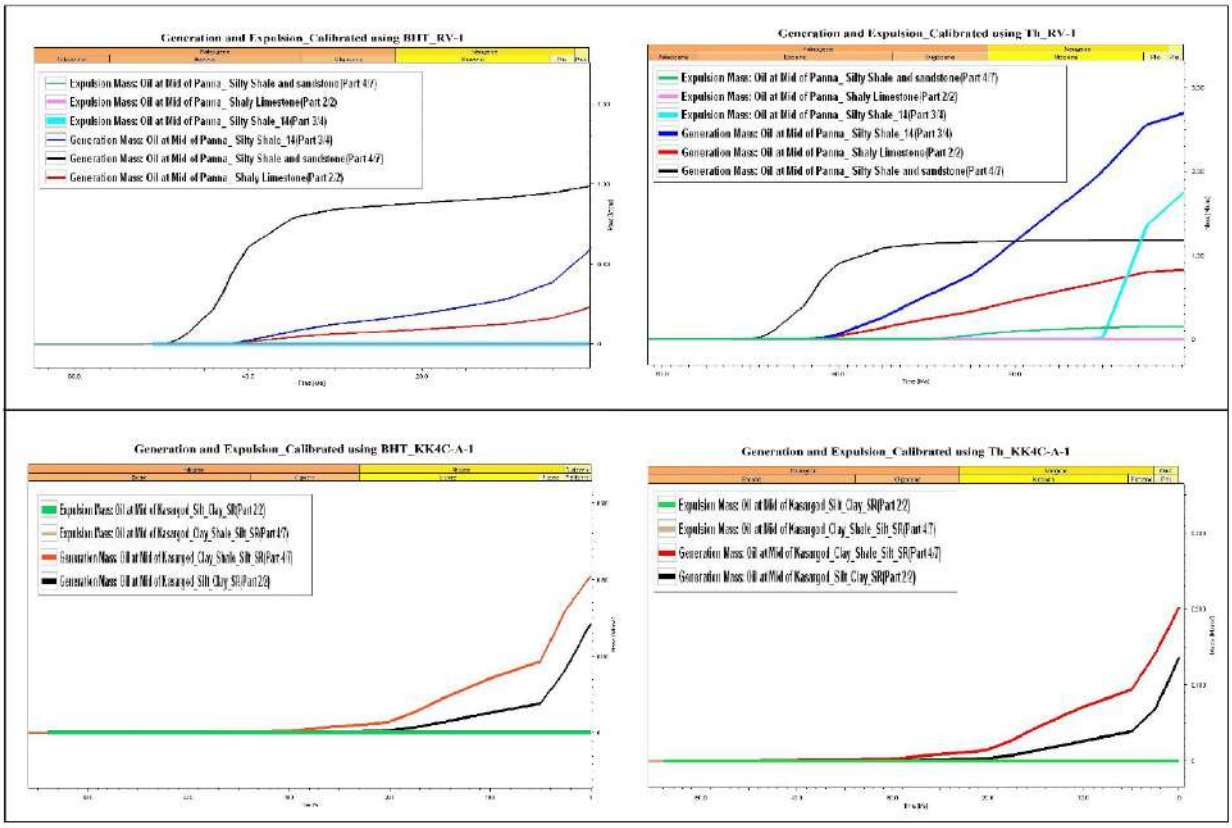

Figure 2. Generation and expulsion of two wells (RV-1 and KK4C-A-1) based on BHT and Th calibrated models.

REFERENCES

Bodnar, R.J. (1990) Petroleum migration in the Miocene Monterey Formation, California, USA: constraints from fluid-inclusion studies. Minerological Magazine 54, 295-304.

Burruss, R.C. (1981) Hydrocarbon fluid inclusions in studies of sedimentary diagenesis. In: Hollister, L.S., Crawford, M.L.Z. (eds) Short Course in Fluid Inclusions: Applications to Petrology. Mineralogical Association of Canada 6, 138-156.

Goldstein, R.H. (2001) Fluid inclusions in sedimentary and diagenetic systems. Lithos55, 159-193.

Nandakumar, V, Jayanthi, J.L. (2016) Hydrocarbon fluid inclusions, API gravity of oil, signature fluorescence emissions and emission ratios: an example from Mumbai Offshore, India. Energy and Fuels30, 3776-3782.

Nandakumar, V., Jayanthi, J.L. (2021) Hydrocarbon Fluid Inclusions in Petroliferous Basins. Elsevier, ISBN: 9780128174173, 1-290.

Evidence of deep-sourced volatiles in the diagenetic evolution of the Aptian carbonates of Santos Basin, Brazil

André L. S. PESTILHO[1], Dorval C. DIAS FILHO[1], Volker LÜDERS[3], Isabela de O. CARMO[1], Anna Eliza S. DIAS[2], Leonardo R. TEDESCHI[1], Bruno R. B. M. de CARVALHO[1], Erica T. de MORAES[1], Delano M. IBANEZ[1], Gustavo GARCIA[2]

[1]*Petrobras Research Centre (CENPES), Av. Horacio Macedo 950, Rio de Janeiro, RJ, Brazil*

[2]*Petrobras Exploration, Av. Henrique Valadares 28, Rio de Janeiro, RJ, Brazil*

[3]*GFZ German Research Centre for Geosciences, Telegrafenberg 14473, Potsdam, Germany*

E-mail: andre.pestilho@petrobras.com.br

The Brazilian Pre-Salt encompasses a large petroliferous province that covers sections of three Cretaceous sedimentary basins: Santos, Campos, and Espírito Santo. Recent studies have unveiled a complex geological history of the Aptian Pre-Salt rocks. It includes: (i) uncommon continental carbonates of debated origin (cf. Wright, 2020); (ii) increasing evidence of both depositional (i.e., travertines; Falcão, 2015) and post-depositional episodes of hydrothermal activity (cf. Wright, 2020 and references there in); and (iii) mantle-sourced CO_2 within the Aptian reservoirs (cf. Santos Neto et al., 2012). Therefore, some questions arisen from the point-of-view of the fluid inclusion studies, such as: (I) Are there any fingerprints of deep-sourced gases trapped in fluid inclusions? (II) Are there any links between any gases in fluid inclusions and hydrothermal events? (III) Lastly, can we suggest a relative timing for gas infill when that is present?

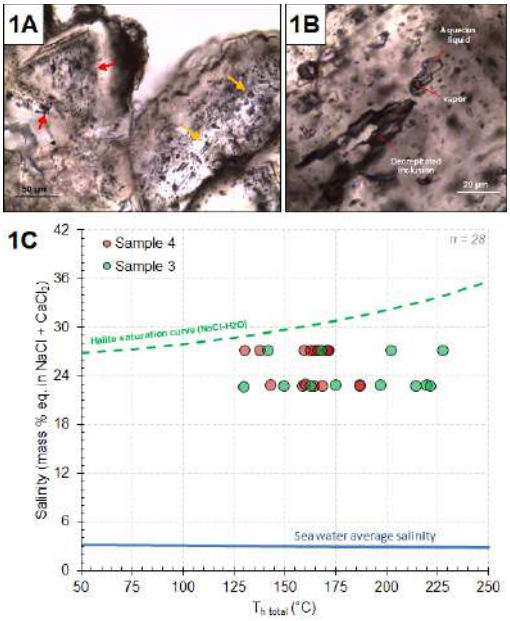

Figure 1. (A) Primary (red arrows) and pseudo-secondary (orange arrows); (B) two-phase (liquid +vapor) aqueous inclusion and decrepitated inclusion; (C) Homogenization temperatures vs. salinity.

In this research, we address such questions through the study of fluid inclusions hosted in late baryte veins (4 samples) from the Aptian carbonates present in SB-1 well in the Santos Basin. Those carbonates are mainly composed by mudstone and laminate facies deposited in a playa lake environment, which overlies travertine rocks (Falcão, 2015). The studied baryte veins cross-cut the playa lake facies carbonates and the underlying travertines. Although magmatic rocks are recognized in many parts of the basin, igneous intrusion are not recognized in the periphery of this well. The methods used in this research included: (i) optical petrography using polarized transmitted light and UV epifluorescence with DAPI filter-set of doubly-polished thick sections; (ii) microthermometry of fluid inclusions; and (iii) on-line extraction and analysis of noble gas composition by isotope mass spectrometry.

The Santos Basin is a very wide margin with a large sedimentary cover (350,000 km^2) originated in the Early Cretaceous as a result of the breakup of the Western Gondwana (Moreira et al., 2007). A rift system widened through time ultimately leading to asymmetric conjugate margins with a notably wide hyperextended domain in Santos Basin (Zálan et al., 2011). During the rifting process, depositional environments changed from a predominantly clastic to a dominantly carbonate setting, capped by an extensive salt layer (up to ~2-3 km thick) at the onset of the Atlantic opening (Mohriak and Fainstein, 2012). Later, the basin evolved to a passive margin with a frankly marine setting from the Aptian onwards. Five major magmatic events are recorded throughout the Santos Basin's geological history (Moreira et al., 2007):(1) ~130 Ma, volcanic economic basement; (2) ~128 Ma, Early Aptian; (3) 118 Ma, Late Aptian; (4) Campanian-Santonian; and (5) Early Eocene.

Baryte cemented fractures comprise post-kinematic cements of a late fracturing event within the playa lake interval. Fluid inclusions hosted in the baryte are mainly primary/pseudo-secondary (Fig. 1A) two-phase (liquid plus vapor) aqueous (Fig. 1B) and oil-bearing inclusions at room temperature. Oil-inclusions are less abundant and they can be divided into two types oil-bearing inclusions based on fluorescence colors: smaller orange (°API < 30) and larger blue/white (°API 40 or higher). Primary inclusions occur in concentric growth zones, whereas pseudo-secondary inclusions are hosted along the main axis of prismatic baryte crystals, but do not cross-cut between different crystals. Fluid inclusion total homogenization temperatures (T_h) display large intervals between minimum and maximum temperatures: (1) aqueous inclusions of 125–230.6 °C, with average ($\bar{x}$) of 174.6 °C and sample standard deviation (σ) of 28 °C (n=42); (2) orange-fluorescent oil inclusions of 69.4–192.6 °C, with $\bar{x}$ of 110.8 °C and σ of 34.5 °C (n=48); (2) blue/white-fluorescent oil inclusions of 68.9–173.4 °C, with $\bar{x}$ of 110.5 °C and σ of 34 °C (n=12).

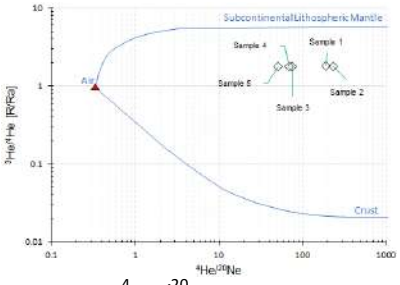

Figure 2. ^{4}He/^{20}Ne vs. ^{3}He/^{4}He (R/Ra) data from pre-salt fluid inclusions, and modelled mixing lines for crust-air (Ballentine & Burnard, 2002), and SCLM-air (Gautheron & Moreira, 2002).

Aqueous inclusions display first melt temperatures (T_m initial) between -45.5 and -44 °C (n=28), and ice-melting temperature (T_m ice) between -24.6 and -23.7 °C, with $\bar{x}$ of -24.1 °C and σ of 0.2 °C (n=28). Few aqueous inclusions showed halite presence, with halite melting (T_m halite) temperature 10.3 and 13.1 °C, with $\bar{x}$ of 11.8 °C and σ of 0.9 °C (n=13). Giving that T_m initial is < -40 °C, inclusions possibly bear Ca-bearing fluids. Therefore, salinities calculated assuming the system $CaCl_2$-NaCl-H_2O, ranged between 22.6–27.1 mass % eq. in NaCl+$CaCl_2$, with average of 24.7 % and σ of 2.2 % (n=28). Some inclusions display significant effects of post-entrapment modification (e.g., decrepitation; Fig. 1C), whilst Th against salinity data clearly indicates stretching (Fig. 1B). The comparison between the Th values and the modelled thermal history shows much higher T_h values than those expected for the samples. Finally, the noble gas composition shows ^{3}He/^{4}He (R/Ra) ratios between 1.77 and 1.81, and ^{4}He/^{20}Ne of 51 and 234, which suggests the contribution of volatiles sourced by subcontinental lithospheric mantle – SCLM (Fig. 2).

The results suggest the coeval presence of hydrocarbons of varied API gravities and brines at the time of entrapment. The absence of boiling features suggests the fluids were trapped in a pressurized environment, and the high salinities might reflect the influx of evaporite-related brines. This association of a pressured environment and high-salinity brines indicate that the baryte veins were formed after the host rock have been buried by the salt layer (~1.5 km thick at the SB-1). In addition, the minimum T_h of aqueous inclusions is above the present-day reservoir temperature (~50 °C) and lower than 200 °C, which reinforces the interpretation of a hydrothermal event that shows temperatures and salinities conditions similar to those of MVT mineral systems. The presence of mantle-sourced volatiles can be interpreted as a deep-source mechanism associated with the hydrothermal event, which could be related to fault zones connecting high temperature deeper domains to the shallower basin domain.

REFERENCES

Ballentine, C. J., Burnard, P. G. (2002) Production, Release and Transport of Noble Gases in the Continental Crust, Reviews in Mineralogy and Geochemistry 47, 481–538.

Falcão, L. C. (2015) Estudo faciológico de um intervalo aptiano do poço SB-1 (Bacia de Santos) e sua comparação com travertinos quaternários de San Juan, Argentina [Master Thesis], Fluminense Federal University.

Gautheron, C., Moreira, M. (2002) Helium signature of the subcontinental lithospheric mantle. Earth and Planetary Science Letters 199, 39–47.

Moreira, J. L. P. et al. (2007) Bacia de Santos. Boletim de Geociências da Petrobras, 15(2), 531–549.

Mohriak, W. U., Fainstein R. (2012) Phanerozoic regional geology of the eastern Brazilian margin. In: Regional Geology and Tectonics: Phanerozoic Passive Margins, Cratonic Basins and Global Tectonic Maps, 222–282.

Santos Neto, E. V. et al. (2012) Origin of CO_2 in Brazilian Basins, in AAPG Search and Discovery, Article #440969.

Wright, V. P. (2020) The mantle, CO_2 and the giant Aptian chemogenic lacustrine carbonate factory of the South Atlantic: Some carbonates are made, not born. Sedimentology 69, 47–73

Zalan et al. (2011) An Entirely New 3D-View of the Crustal and Mantle Structure of a South Atlantic Passive Margin – Santos, Campos and Espírito Santo Basins, Brazil, in AAPG Search and Discovery Article #30177.

A fluid inclusion outlook on the petroleum migration of the Cretaceous Potiguar Basin, Brazilian Equatorial Margin

André Luiz Silva PESTILHO[1], Lena Virgínia Soares MONTEIRO[2]

[1]*Petrobras Research Centre (CENPES), Av. Horacio Macedo 950, Rio de Janeiro, RJ, Brazil*

[2]*Institute of Geosciences, University of São Paulo, Rua do Lago 562, São Paulo, SP, Brazil*

E-mail: andre.pestilho@petrobras.com.br

Fluid inclusions have long been a recurring tool in the petroleum industry, providing relevant information on the timing, temperature, pressure, and compositional constrains of petroleum systems (see Volk and George, 2019 and references therein). Its application serves both green fields and mature proliferous provinces alike, such as the case of the Potiguar Basin – a historical petroleum province located in the Brazilian Equatorial Margin (BEM) and the subject of this study (Fig. 1).

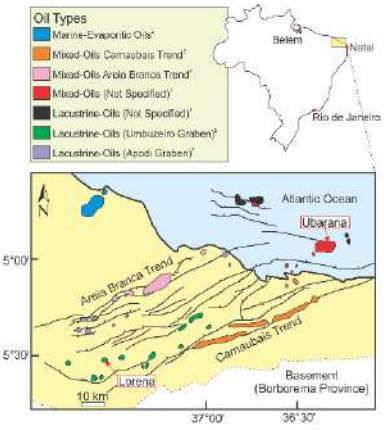

Figure 1. Potiguar Basin map: major rift structures, oil types, and the location of Lorena and Ubarana fields (Pestilho et al. 2018b and references therein).

The Potiguar Basin encompasses about 6 km thick sedimentary cover deposited during Cretaceous as a result of the tectonic break-up of the Western Gondwana (Pestilho, 2018 and references therein). The petroleum systems of the Potiguar Basin display a complex evolution, which includes long-range migration, mixed lacustrine-marine source-rocks, and biodegradation (Trindade et al., 1992). The reservoirs within the Potiguar Basin were chiefly charged by two source-rock units: (i) the Neocominian Pendência Formation, deposited in lacustrine settings; and (ii) the Aptian Alagamar Formation, that was deposited in the transition of continental to marine sedimentary settings (Trindade et al., 1992). The lacustrine oils sourced by the Pendência shales charged the Pendência sandstones in the southern section of the basin, while the Alagamar marine to mixed-source oils were mainly responsible by the accumulations found in the fluvial to deltaic clastic deposits of the Albian-Cenomanian Açu Formation located in both offshore and onshore (Trindade et al., 1992). Partial information on the onset of oil charge of these reservoirs were available at the time of this study, with estimation mostly derived from basin modelling studies. The complexity of the petroleum systems of the Potiguar Basin, and the renewed interest in the exploration within the BEM (Silva et al., 2021) provided an opportunity for the application of fluid inclusions in the understanding of the timing and the physical constraints involved in the charge history of the petroleum traps. The information provided by the reconstruction of the charge history of the Potiguar Basin may serve as an analogue to understand similar petroleum systems in the adjacent sedimentary basins at the BEM (Silva et al., 2021).

Here we summarize the main results and insights provided by the first systematic research using fluid inclusions (Pestilho, 2018; Pestilho et al., 2018a, 2018b, 2021) to address the major petroleum systems of the Potiguar Basin, using several tools: epifluorescence petrography, oil fluorescence spectrophotometry, petroleum biomarkers, confocal scanning laser microscopy, basin modelling, and PVT modelling of fluid inclusions. The major goal of this study was to constrain the early petroleum migration and address its association with the diagenetic environment at the onset of the oil charge history. With that major goal, two oilfields were chosen to as target areas: (1) the onshore Lorena (reservoir: Pendência Formation), and (2) the offshore – Ubarana (reservoir: Açu Formation; and the adjacent carbonates from the Ponta do Mel Formation) oilfields.

In the Lorena oilfield, fluid inclusion assemblages consisted of two-phase (liquid plus vapor or L-V) petroleum inclusions entrapped during the mesodiagenesis of the arkose hyperpycnites of the Pendência Formation: (I) in quartz, as both primary inclusions in syntaxial cement and secondary inclusions in detrital grains, and (II) in albite intragranular cement as primary inclusion. As for the Ubarana area, in the Açu Formation two-phase (L-V) secondary petroleum inclusion were trapped in quartz pebbles of fan-delta conglomerate pebbles during the late

mesodiagenesis, whilst in Ponta do Mel Formation shallow shelf carbonates, two-phase (L-V) petroleum and aqueous inclusions are hosted in saddle dolomite veins originated during late mesodiagenesis.

Both source and maturity parameters from biomarkers indicate that the Pendência and Açu inclusion oils correlate with reservoir oil extracts. The Pendência inclusion oils are similar to the lacustrine oils sourced by the Pendência Formation (ex., low C_{24}-tetracyclic terpane/C_{23}-tricyclic terpane ratio and, low gammacerane/C_{30}-hopane ratio), whereas the Açu inclusion oil displays closer biomarker signature to that of the Alagamar Formation mixed oils (ex., low tricyclic terpanes/total hopanes ratio, intermediate gammacerane/C_{30}-hopane ratio). However, the oil from fluid inclusions of the Ponta do Mel has characteristics of the Alagamar Formation lacustrine organic facies (ex., high tricyclic terpanes/total hopanes ratio, low gammacerane/C_{30}-hopane ratio). The absence of mixed oils in the Ponta do Mel suggests an earlier lacustrine oil migration through the carbonate fractures prior to the main infill of mixed-oils in the Ubarana oilfield.

Fluid inclusion microthermometry, confocal scanning laser microscopy and basin modelling suggest that the initial filling of the Lorena reservoir occurred during the late rifting stage (Barremian and Early Aptian; ca. 129–124 Ma) at 62.7–80.6 °C (11–16.8 MPa) (Fig. 2). In the Ubarana oilfield, hydrothermal fluids migrated with the petroleum during the reservoir initial filling. The total homogenization temperatures for both Açu (Th_{mode} = 124–128 °C) and Ponta do Mel (Th_{mode} = 115–130 °C) are higher than the past and present-day reservoir temperature (present-day reservoir temperature = 110 °C) (Fig. 2).

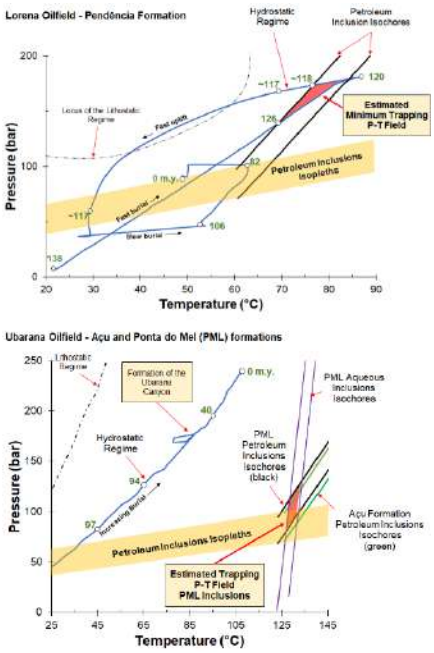

Figure 2. P-T diagrams comparing thermal histories, and fluid inclusions isochores for the Lorena and Ubarana oilfields (Pestilho et al. 2021).

Isochoric modelling of saddle dolomite-hosted fluid inclusions from the Ponta do Mel Formation indicates trapping temperatures between 128.9 and 133.1 °C and pressures between 10.6 and 12.9 MPa. Temperatures and equivalent salinities (mode interval between 16 and 20 mass % equivalent in $NaCl+CaCl_2$) of aqueous inclusions hosted in saddle dolomite are alike the fluid inclusions trapped in hydrothermal minerals in Pb-Zn Mississippi Valley-Type deposits. Finally, no specific timing can be suggested for the hydrothermal event in Ubarana Oilfield. However, this atypical (hydrothermal) petroleum system could be linked to two possible scenarios: (i) the onset of petroleum migration of the Alagamar Formation during the Cenozoic Macau (ca. 48–8.8 Ma) magmatic event; or (ii) an earlier activity of the petroleum system, prior to the peak oil generation (50–10 Ma).

REFERENCES

Pestilho, A.L.S. (2018) Aplicação de inclusões fluidas à reconstrução da história de migração de hidrocarbonetos na Bacia Potiguar, RN [Ph.D. Dissertation]. Universidade de São Paulo, Brazil, 485 p.

Pestilho, A.L.S. et al. (2018a) Hyperpycnal-fed lacustrine turbidites in rift basins: Facies analysis and diagenesis of the Early Cretaceous Pendência Formation, Potiguar Basin, Brazil, J. of South American Earth Sciences 87, 4-24.

Pestilho, A.L.S. et al. (2018b) Linking the geochemistry of crude oils and petroleum inclusions in the Ubarana and Lorena oilfields, Potiguar Basin, Brazilian Equatorial Margin, Organic Geochemistry 124, 133-150.

Pestilho, A.L.S. et al. (2021) Unraveling the early petroleum migration of the Potiguar Basin, Brazil: Constraints from fluid inclusions of the Ubarana and Lorena oilfields, Marine and Petroleum Geology 132, 105200.

Silva, E.B., et al. (2021), Exploration plays of the Potiguar Basin in deep and ultra-deep water, Brazilian Equatorial Margin, J. of South American Earth Sciences 111, 103454.

Trindade, L. A. F. et al. (1992) Petroleum migration and mixing in the Potiguar Basin, Brazil, AAPG Bulletin, 76(12), 1903-1924.

Volk, H., George, S.C. (2019) Using petroleum inclusions to trace petroleum systems – A review, Organic Geochemistry 129, 99-123.

Raman Spectroscopic Properties of Aqueous Chloride Solutions: Chlorides of Alkali, Alkaline Earth, and First Row Transition Metals.

Spencer L. Poulette[1], Matthew Steele-MacInnis[1]
[1]*University of Alberta, Department of Earth and Atmospheric Sciences*
E-mail: spoulett@ualberta.ca

Raman spectroscopy has been used as a method to non-destructively perform analyses on fluid inclusions for several years. This technique has continually evolved to allow for the direct estimation of salinity within fluid inclusions without the need for specialized microthermometry stages or knowledge of complex chemical systems. However, the technique has typically lacked the ability to concretely characterize the composition of the fluid. Using a series of 19 salts, we present data regarding the identification of chloride salts within aqueous solutions and compare the salinity estimates from Sun *et al*, 2010 with those gained from this study.

This study is performed using a Horiba Scientific LabRam HR Evolution Raman spectrometer with a 532nm laser operating at 100% of its 1.5mW power. The spectrometer was set to collect windows from 50 to 4000 cm^{-1} with exposures of 30 seconds for 3 collections each on a grating of 1800 slits/cm. The spectrometer was outfitted with a cuvette holder, in which a quartz glass cuvette was placed containing an aliquot of solution. In total, 19 salts were analyzed from the alkalis, alkaline Earth, and transition metal groups.

It was found that 12 of these 19 salts were identifiable within solution due to the presence of new peaks within the Raman spectrum. These peaks grew in intensity as concentration increased, indicating that these were interactions of the salt within the water network. These new peaks have been theorized to be the presence of ion pairs or coordination complexes. These complexes can be categorized as weak or strong, depending on the individual compound being investigated. The strength of the ion pairing was delineated by the shape of the peak as well as the intensity of the peak relative to the signal for water, where strong ion pairs had sharp high intensity peaks and weak ion pairs have broad low intensity peaks. Compounds with strong ion pairs are $CuCl_2$, $FeCl_3$, $NiCl_2$, $SnCl_2$, and $CoCl_2$. These compounds form sharp peaks at low wavenumber on the Raman spectrum, likely indicating the presence of tetrahedrally-coordinated complexes of the form XCL_3, wherein X denotes the cation in solution. These ion pairs are stable in solution, and have distinctive peaks as noted in table 1.

In addition to the presence of ion pairs, we investigated the effects of different salts on the OH-stretching region of water. The ratio of symmetric stretching peaks to asymmetric stretching peaks has been calibrated to be used as an estimate of molarity of chlorine held in solution (Sun *et al*, 2010). We found that differing peak models can have a profound effect on this estimate. Whilst Sun *et al*, 2010 uses a two-peak model, our fitting model of five peaks still follows the trend of increasing molarity with increasing symmetric/asymmetric OH-stretching ratios. However, salts which form strong ion pairs in solution lead to inaccurate salinity estimates, as the symmetric/asymmetric OH-stretching ratios are disrupted by the presence of these ion pairs. This necessitates taking a broad spectral scan of fluids of unknown composition where one might expect salts which form high strength ion pairs.

REFERENCES

Sun, Q., Zhao, L., Li, N., & Liu, J. (2010). Raman spectroscopic study for the determination of Cl− concentration (molarity scale) in aqueous solutions: Application to fluid inclusions. *Chemical Geology*, *272*(1–4), 55–61. https://doi.org/10.1016/j.chemgeo.2010.02.004

Table 1. Chloride salts and compounds used in experiments with magnitude of increase of concentration between each experiment. New peaks given for each salt if seen in spectra.

Compound	Salt	Concentration Range (wt%)	Measurement interval (wt%)	New peaks?
HCl	$HCl_{(aq)}$	0 - 37	5	X
LiCl	LiCl anhydrous	0 - 45	2	X
NaCl	NaCl anhydrous	0 - 26	1	-
KCl	KCl anhydrous	0 – 25	1	-
RbCl	RbCl anhydrous	0 – 47	10	-
CsCl	CsCl anhydrous	0 - 65	5	-
$MgCl_2$	$MgCl_2$ hexahydrate	0 - 34	2	X
$CaCl_2$	$CaCl_2$ dihydrate	0 - 43	2	-
$SrCl_2$	$SrCl_2$ hexahydrate	0 - 34	10	-
$BaCl_2$	$BaCl_2$ dihydrate	0 - 25	5	-
$MnCl_2$	$MnCl_2$ tetrahydrate	0 - 39	2	X
$FeCl_2$	$FeCl_2$ tetrahydrate	0 - 40	5	X
$FeCl_3$	$FeCl_3$ anhydrous	0 - 47	10	X
$CoCl_2$	$CoCl_2$ hexahydrate	0 - 33	2	X
$NiCl_2$	$NiCl_2$ hexahydrate	0 - 30	2	X
$CuCl_2$	$CuCl_2$ anhydrous	0 - 43	2	X
$ZnCl_2$	$ZnCl_2$ anhydrous	0 - 80	10	X
$SnCl_2$	$SnCl_2$ anhydrous	0 - 45	2	X
NH_4Cl	NH_4Cl anhydrous	0 - 28	2	X

Determining Pressure and Temperature of Gold-Related Fluid Inclusion Formation at Salmita Mine, NWT

Spencer L. Poulette[1], Matthew Steele-MacInnis[1]
[1]*University of Alberta, Department of Earth and Atmospheric Sciences*
E-mail: spoulett@ualberta.ca

Salmita Mine is located 240 kilometers Northeast of the city of Yellowknife, Northwest Territories. The mine was active from 1983 to 1987, during which time it produced 179,000 ounces of gold at an average grade of 27 grams/ton, making it one of the most prolific orogenic gold mines of its time. The mine operated out of a single sub-vertical quartz vein occurring at the contact of mafic volcanics and shale, named the B-vein which ranged in width up to 20 meters and grades up to 120 grams/ton. Approximately 50 meters to the East is another vein, hosted within felsic volcanics, named the T-vein. This vein was not exploited due to its uneconomic average grade at the time of 17 grams/ton. Samples were received from the Northwest Territories Geologic Survey and subsequently analyzed by optical microscopy, Raman spectroscopy, scanning electron microscopy (SEM), and electron microprobe analyses (EPMA).

Regionally, the mine is situated in the large Northwest-Southeast trending Courageous Lake Greenstone Belt, which is dated to 2.5 Ga (Adam, 2016). This belt is dominantly composed of successions of shallow sedimentary rocks, mafic volcanics, and felsic volcanics which host Salmita Mine. The samples of both veins are composed of highly strained quartz with minor amounts of sulfides such as pyrrhotite, pyrite, arsenopyrite, sphalerite, marcasite, and galena. These samples also contain up to 1 weight percent Tungsten hosted in scheelite. Gold often occurs in these veins as free milling grains in close association with arsenopyrite and pyrite. These sulfides contain no detectable gold above 40 ppm as seen in results from EPMA analyses.

In addition to mineralized veins, crosscutting non-mineralized veinlets can be seen in most samples. These veins are composed of open space-filling quartz, growing inward from the vein wall, with multiple generations of pyrite overgrowths. The last phase of these veins is dolomite, filling in the space between euhedral quartz as a cryptocrystalline phase. Fluid inclusions within the cores of quartz grains are low salinity (<3 wt%). These veins are interpreted to be the last phase of mineralization in the deposit, possibly due to decompression during exhumation.

Fluid inclusions in the T-vein display low degrees of shearing, often preserving primary fluid inclusions within relict grains. Fluid inclusions in these relict grains often contain a low-density aqueous fluid, CO_2, methane, graphite, and muscovite (Figure 1). Cathodoluminescence was performed on primary fluid inclusion assemblages hosted within relict quartz grains. We found that there was no evidence for fluid inclusion migration or integration of trace elements from the host quartz into fluid inclusions. B-vein textures are indicative of a high degree of shearing. These textures include decrepitation of fluid inclusions, evidence of fluid leakage, development of subgrains, and undulose extinction. Fluid inclusions in this vein are rarely primary due to the high degree of shearing destroying most fluid inclusions. Breached inclusions are evidence by the large amount of muscovite inclusions in parallel trails within quartz grains.

Graphite in inclusions from the T-vein were analyzed by Raman spectroscopy for temperatures of formation, which was found to be approximately 325°C. Additionally, CO_2 densimetry was performed using a calibration equation for the Raman spectrometer at the University of Alberta. The density within these inclusions of CO_2 is 0.76 grams/cm^3, indicating a liquid state. Using the combination of graphite microthermometry and CO_2 densimetry, we estimate the pressure of formation of these inclusions to be 1400 ± 100 bars. This is consistent with a burial depth of 3 to 4.5 kilometers, making this a shallow orogenic gold deposit.

Figure 5. Muscovite and graphite-bearing inclusions from the T-vein at Salmita Mine.

REFERENCES

Adam, Marcus A., "Gold Mineralisation at the FAT Deposit, Courageous Lake Greenstone Belt, Northwest Territories, Canada" (2016). Electronic Thesis and Dissertation Repository. 3640. https://ir.lib.uwo.ca/etd/3640.

Fluid inclusion study of Ag and Sn bearing hydrothermal veins along the shear zone of Main Central Thrust in Himachal Himalaya, India.

Shruti Rana[1], Rajesh Sharma

Wadia Institute of Himalayan Geology, Dehra Dun – 248 001, India
E-mail: [1]shrtrn5@gmail.com

The in-sequence growth and the southward propagation of the ~50-55 Ma Himalayan orogenic belt towards the foreland provides a distinctive geological setting to understand the surficial and landscape evolutionary processes and formation of different ore occurrences/deposits. The inverted and ultra-high-pressure metamorphism along with the active thrust zones are the most enigmatic features of this complex system. These thrust zones are expected to be the promising ore bearing locations. One such occurrence of the polymetallic sulphides is found along the Main Central Thrust shear zone, boundary between Lesser Himalayan metasedimentaries and the Higher Himalayan crystallines Himachal Himalaya. This ~5 meter thick, polymetallic sulphide bearing hydrothermal quartz vein is focused to understand the ore forming fluid and thereby the ore genesis. Carbonaceous material is also present in the mineralized shear zone.

The mineral assemblage includes arsenopyrite, pyrite, galena and chalcopyrite as main primary minerals, whereas the scorodite and anglesite are important secondary minerals. Arsenopyrite and pyrite are enriched in Cu, Pb, Ag and Sn. Primary fluid inclusions in host quartz veins are classified into monophase aqueous, monophase carbonic, biphase liquid rich aqueous inclusions, biphase vapour rich inclusions, and polyphase type of fluid inclusions. These primary fluid inclusions represent syn ore mineralisation fluid. The other set of secondary fluid inclusions contains only monophase and biphase aqueous fluid inclusions. Micro Raman spectroscopy confirms that the composition of primary fluid system involves gas and liquid CO_2, CH_4 and N_2. The fluid inclusion assemblage (FIA) including liquid rich and vapour rich fluid inclusions attribute the fluid immiscibility and/or boiling during the entrapment. The presence of liquid gas meniscus at room temperature points to the low density of CO_2. The homogenization temperatures of the primary biphase and most polyphase inclusions ranges from ~300°C to < ~450°C, and the salinity is estimated to be less than ~ < 12 equi. Wt% NaCl. The source of sulphur in the hydrothermal ore forming fluid is interpreted from the mixed source, whereas the carbonaceous material in the vicinity of ore mineralization is entirely sedimentary metamorphosed carbon.

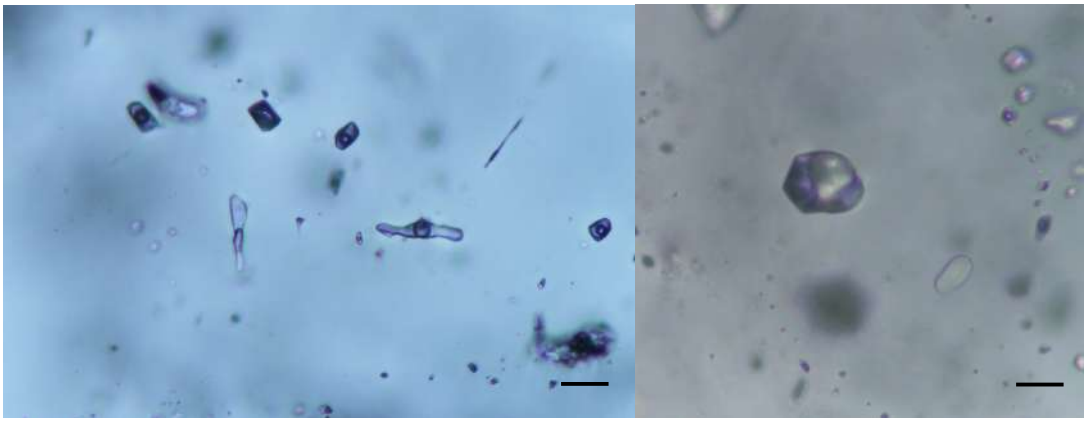

Figure 1. These two photomicrographs show the FIA on left side and the primary polyphase fluid inclusion on right.

Ore forming fluid characteristics of orogenic gold deposits from Saqqez–Sardasht–Piranshahr gold field, north-west of Iran

Shojaeddin Niroomand[1], Hossein Ali Tajeddin[2], Majid Soleymani[1], Dunya Maronsi[1]

[1] *Department of Earth Sciences, Faculty of Sciences, Tehran University, Tehran 14155-64155, Iran*
[2] *Department of Geology, Faculty of Basic Sciences, Tarbiat Modarres University, Tehran, Iran*
E-mail: Soleymani.Majid@ut.ac.ir

One of western Iran's principal gold-bearing zones is the Sanandaj-Sirjan Zone (SSZ), which hosts a comprehensive range of gold deposits. The Saqqez–Sardasht–Piranshahr zone is a NE-trending goldfield belt in the northern part of the SSZ, consisting of mafic to intermediate metavolcanic and metasedimentary rocks. The majority of gold deposits and occurrences in the Saqqez–Sardasht–Piranshahr zone are linked to strongly pyritized, silicified, and sericite alteration and originated in greenschist-facies metamorphic rocks. The orebodies occur mainly as veins, irregular, lenticular bodies in altered rocks (Heidari, 2004; Aliyari et al., 2007). Numerous gold mineralizations have reportedly been discovered in the Sanandaj-Sirjan Zone provided by the Iranian Geological Survey (Tajeddin, H.A., 2008). According to earlier investigations, the orogenic gold resources of the region include; Qolqoleh, Kervian, Qabaqlojeh, Hamzeh Qaranein, Kasnazan, Shovey, Alut, Mirgeh Naghshineh (Aliyari et al., 2007, 2009, 2012; Asghari et al., 2018; Tajeddin, H.A., 2011), Kharapeh (Niroomand et al., 2011), Zinvinjian (Asadi et al., 2018).

Based on the fluid inclusion data of Zinvinjian, Kharapeh, Shovey, Kasnazan, Hamzeh Qaranein, and Qabaqlojeh, the ore-forming fluid has been interpreted. Zinvijian Cu–Pb–Zn–Au deposit occurs in veins within the Cretaceous metamorphosed limestone and dolomite, schist, and metavolcanic rocks. Two stages of mineralization have been recorded: early-stage polymetallic sulfides–quartz and late–stage pyrite–quartz veins. These have demonstrated three types of fluid inclusions in ore-related quartz veins. The early–stage quartz Fluid inclusions homogenized at temperatures ranging from (197–300°C) with salinities of (2.5–15.2 wt.% NaCl). In contrast, the late–stage quartz veins Fluid inclusions presented homogenization temperatures ranging between (192 and 210°C) with salinities of (0.2–2.7 wt.% NaCl). Meanwhile, Kharapeh orogenic gold deposit is an epizonal orogenic gold formed during the Cretaceous-Tertiary Zagros orogeny. Mineralization is mainly recognized in veins and breccia zones. Hydrothermal alteration mainly consists of silicification, sulfidation, chloritization, sericitization, and carbonatization. Fluid inclusion data suggest mineral deposition at temperatures of at least (220–255°C) and depths of at least 1.4–1.8 km from an H2O–CO2±CH4 fluid of relatively high salinity (12–14 wt.% NaCl), which may reflect metamorphism of passive margin carbonate sequences. The Hamzeh Qaranein gold mineralization's main part coincides with a post-Cretaceous granitoid intrusion. Mineral deposition from a CO2-bearing fluid of relatively low salinity (0.6 to 7.65% NaCl) at temperatures between (138 and 309 °C) is suggested by fluid inclusion data. In addition, the Ghabaqloujeh gold deposit consists of schist, phyllite, and marble volcanic-sedimentary phases from the Precambrian and Cretaceous that were intruded by granitoid rocks. According to studies on fluid inclusion, the homogenization temperature ranges from (162 to 255°C), while salinity is (0.6 to 17.08% NaCl). The study demonstrates the mixing of an isothermal fluid with low salinity and a hydrothermal fluid with moderate temperature, which can be accomplished by a combination of dilution and mixing processes. A series of metamorphosed volcano-sedimentary rocks from the Cretaceous era, containing andesite lavas, metamorphosed andesibasalts, schist, and phyllite, is where the Shovey gold deposit is found. This deposit's mineralization is developed as a vein in limestone host rock. Fluid inclusion data of quartz and sphalerite reveal that ore fluids have a homogeneity temperature of (165 to 340 °C), with a salinity of (0.02 to 9.02%). Moreover, the Kasnazan gold deposit is located in a group of metamorphosed volcanic-sedimentary rocks from the Precambrian and Cretaceous eras, comprising marble, schist, and phyllite that are cleaved by granitoid masses. The syenite quartz bulk is the primary host of gold mineralization. A series of silica, sericite, carbonate, and sulfide minerals are present along with mylonitic-ultramylonitic fibers in the highly metamorphosed and altered portions of syenite quartz mass that make up gold-bearing ores. Studies of fluid inclusions on quartz from gold-bearing ores reveal that the homogenization temperature of mineralization fluids is between (137.4 - 240.5 °C), while the salinity is between (1.16 to 12.06%).

Based on the evidence provided, the Saqqez–Sardasht–Piranshahr zone of the northern Sanandaj-Sirjan contains a significant orogenic gold resource. It is one of the three parallel belts related to the major tectonic events associated with the New-Tethys development and movement of the Arabian Plate toward the Iranian Plate during the Cretaceous. The main magmas and their derivative fluids from the Early Cretaceous were concentrated at

dilational locations and fault junctions at the SSZ, causing orogenic-type gold deposits. Accordingly, most mentioned deposits are primarily found in altered rocks as veins. The Fluid inclusion data studied on various orogenic gold deposits in the mentioned region have been collected and interpreted. Although numerous other orogenic gold occurrences in the area still need detailed fluid inclusion research. However, based on the mentioned ore deposits, the average salinity and homogenization temperature were concluded as respectively (0.02 % -18 % NaCl) and 137°C to 340°C. These indications vectors toward a characteristic of a typical orogenic gold deposit.

REFERENCES

Aliyari, F., Rastad, E. and Mohajjel, M. (2012), Gold Deposits in the Sanandaj–Sirjan Zone: Orogenic Gold Deposits or Intrusion-Related Gold Systems?. Resource Geology, 62: 296-315.

Aliyari, F., Rastad, E., and Zengqian, H., (2007), Orogenic gold mineralization in the Qolqoleh deposit, Northwestern Iran. Journal of Resource Geology, 57: 269–282.

Aliyari, F., Rastad, E., Mohajjel, M., and Arehart, G.B., (2009), Geology and geochemistry of D-O-C isotope systematics of the Qolqoleh gold deposit, Northwestern Iran: Implications for ore genesis. Ore Geology Reviews, 36(4): 306–314.

Asghari, G., Alipour, S., Azizi, H., and Mirnejad, H., (2018), Geology and mineral chemistry of gold mineralization in Mirge-Naqshineh occurrence (Saqez, NW Iran): Implications for transportation and precipitation of gold. Acta Geologica Cinica (Eng; Edition), 92(1): 210–224.

Asadi, S., Niroomand, S., Moore, F., (2018), Fluid inclusion and stable isotope geochemistry of the orogenic–type Zinvinjian Cu–Pb–Zn–Au deposit in the Sanandaj- Sirjan metamorphic belt, Northwest Iran. J. Geochemical Explor. 184, 82–96.

Heydari, S.M., (2004), Mineralography, geochemistry and fabric of gold mineralization in Kervian ductile shear zone, SW Saqez, Kurdistan Province. MSc. Thesis, Tarbiat Modarres Univ., Faculty of Sciences (in Farsi).

Niroomand, Sh., Goldfarb, R.J., Moore, F., Mohajjel, M., and Marsh E.E., (2011), The Kharapeh orogenic gold deposit: Geological, structural, and geochemical controls on epizonal ore formation in West Azerbaijan Province, Northwestern Iran. J. Mineralium Deposita 46, 409–428.

Tajeddin, H.A., (2008), Exploration and introduction of the gold mineralization at the Southern Ghabaghloujeh area (SW of Saqqez, Kurdistan). Geological Survey and Mineral Exploration of Iran, Internal report 35p.

Tajeddin, H.A., (2011), Ore controlling parameters of gold mineralization in the Saqqez-Sardasht metamorphosed area, NW of Sanandaj-Sirjan metamorphic zone. Ph.D thesis.

Muscovite crystals in carbonic fluid inclusions, Red Lake mine trend, Ontario, Canada

Marko A. Szmihelsky[1], Matthew Steele-MacInnis[1], Guoxiang Chi[2], Spencer L. Poulette[1]
[1]*Department of Earth and Atmospheric Sciences, University of Alberta, 1-26 Earth Sciences Building, Edmonton, Alberta, T6G 2E3, Canada*
[2]*Department of Geology, University of Regina, Regina, Saskatchewan, S4S 0A2, Canada*
E-mail: mszmihel@ualberta.ca

The Red Lake gold deposit, a high-grade greenstone-hosted orogenic gold deposit in Ontario, Canada, is a classic example of an orogenic gold deposit in which fluid inclusions are almost entirely carbonic, with very little to no H_2O (Chi et al., 2006). A number of models have been proposed to explain the dominance of pure CO_2 inclusions in certain orogenic gold deposits: 1) the occurrence of an H_2O-poor gold mineralizing fluid (Schmidt Mumm et al., 1997; Xavier and Foster, 1999), 2) fluid unmixing (Garba and Akande, 1992; Tarnocai, 2000) and 2) the preferential leakage of H_2O during post-entrapment modification (Klemd, 1998). Here, we present results from an ongoing fluid inclusion study of the Campbell-Red Lake deposit within the Red Lake mine trend.

In this study, we utilized high-resolution micro Raman spectroscopy to analyze carbonic fluid inclusions from Red Lake. The fluid phase assemblage of these inclusions contains CO_2 with variable CH_4 and N_2, and no H_2O. However, Raman point analyses and 2D/3D maps of these inclusions uncovered the near-ubiquitous presence of muscovite crystals hosted in carbonic inclusions (Fig. 1), and as abundant mineral inclusions in quartz. The origin of muscovite in carbonic inclusions is unclear, but a few possibilities exist: 1) muscovite was co-trapped with a carbonic fluid, 2) muscovite is a daughter mineral of these inclusions, and 3) muscovite is a product of post-entrapment modification of the fluid inclusions and quartz. Muscovite ($KAl_2(AlSi_3O_{10})(OH_2)$) contains H_2O in its crystal structure, and could represent a sink into which residual H_2O was sequestered if muscovite was crystallized post-trapping. Therefore, insights into the origin of muscovite will provide clues as to whether or not H_2O was present in the mineralizing fluid at Red Lake. Future goals of this study are to investigate whether muscovite is a product of post-entrapment modification by using cathodoluminescence and electron microprobe analysis, and to employ the same methods used here to investigate carbonic inclusions in the Ashanti Belt, Ghana.

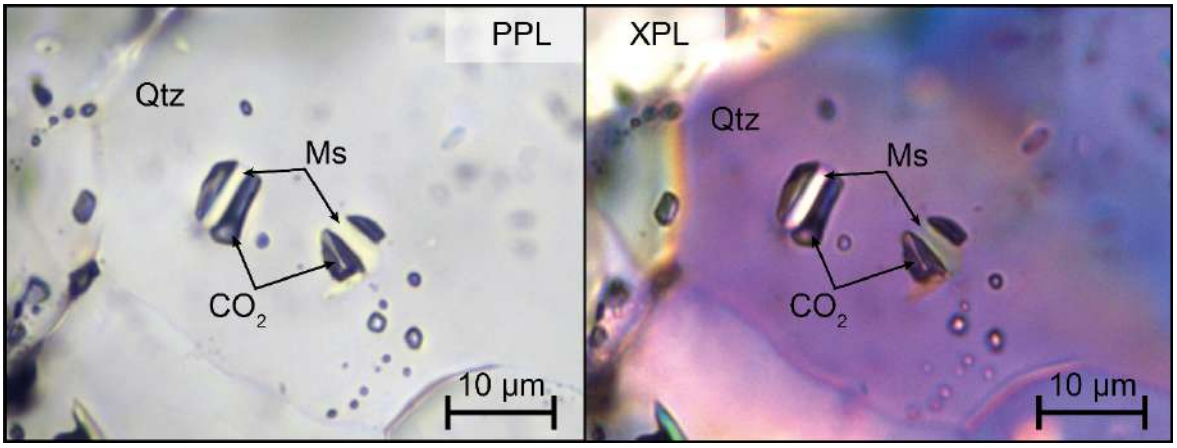

Figure 6. Carbonic inclusions hosting muscovite crystals. The image on the left is in plane-polarized light (PPL), and the right image is in cross-polarized light (XPL). Qtz = quartz, Ms = muscovite.

REFERENCES

Chi, G., Dubé, B., Williamson, K., Williams-Jones, A. (2006) Formation of the Campbell-Red Lake deposit by H_2O-poor, CO_2-dominated fluids. Mineralium Deposita, 40, 726-741.
Garba, I., Akande, S.O. (1992) The origin and significance of non-aqueous CO_2 fluid inclusions in the auriferous veins of Bin Yauri, northwestern Nigeria. Mineralium Deposita, 27, 249-255.

Klemd, R. (1998) Comment on the paper by Schmidt Mumm et al. High CO_2 content of fluid inclusions in gold mineralizations in the Ashanti Belt, Ghana: a new category of ore forming fluids? (Mineralium Deposita, 32, 107-118). Mineralium Deposita, 33, 317-319.
Schmidt Mumm, A., Oberthür, T., Vetter, U., Blenkinsop, T.G. (1997) High CO_2 content of fluid inclusions in gold mineralizations in the Ashanti Belt, Ghana: a new category of ore forming fluids? Mineralium Deposita, 32, 107-118.
Tarnocai, C. (2000) Archean gold mineralization at the Campbell mine, eastern Red Lake greenstone belt, western Superior Province of Canada. Ph.D. thesis, University of Ottawa, 227 p.
Xavier, R.P., Foster, R.P. (1999) Fluid evolution and chemical controls in the Fazenda Maria Preta (FMP) gold deposit, Rio Itapicuru Greenstone Belt, Bahia, Brazil. Chemical Geology, 154, 133-154.

Evidence for infiltrative contact metasomatism between silicate melts and carbonates at Chating, China

Xinyue Xu[1,2], Matthew Steele-MacInnis[2], Xiaochun Xu[1], Marko Szmihelsky[2]

[1] *School of Resources and Environmental Engineering, Hefei University of Technology, 193 Tunxi Road, Hefei, 230009, China*

[2] *Department of Earth and Atmospheric Sciences, University of Alberta, 1-26 Earth Sciences Building, Edmonton, T6G2E3, Canada*

E-mail: xxu20@ualberta.ca

Calc-silicate skarns (endoskarns) are considered natural evidence for magma-carbonate interaction via decarbonation of carbonate and desilication of silicate melts (Lentz, 1999; Gaeta et al., 2009; Carter and Dasgupta, 2016; Whitley et al., 2020). Lentz (1999, 2005) proposed that crustal carbonate melts can be produced via carbonate anatexis during high-temperature contact metamorphism, and emphasized infiltrative skarn formation and its association with mineralization. However, the related petrological process lacks more direct evidence (such as melt inclusion), and the interplay between mineralized systems and infiltrative skarn formation remains unclear. Here, we present a fluid-melt inclusion study of the copper-gold mineralized system containing endoskarns at Chating (eastern China) to provide a natural example of infiltrative skarn formation.

Our results show that the calcium-silicate minerals at Chating crystallize from homogeneous Ca-rich sulfate melts, while Na-K-Fe-rich salt melts are prevalent in this system. Thus, we contend that interactions between silicate melts and carbonates involve the following possible events. First, partial melting of carbonates and/or evaporite occurs in an H_2O-rich shallow-emplaced magmatic system via volatile fluxes (Figure 1A), forming a Ca-rich sulfate melt-fluid two-phase flow system. Second, the carbonate melt acts as a barrier to fluid circulation. In this scenario, large-scale marble formed by thermal metamorphism replaces the exoskarn aureole formed by contact metamorphism. Marble shell acts as a barrier to further assimilation of carbonate wall rocks, however, assimilation and partial melting of marble appear to occur continuously (Figure 1B). Third, Infiltrative contact metamorphism occurs as the Ca-rich sulfate melts migrate away, promoting more carbonate melting via decarbonation. Silicate melts react with the widespread carbonate melts and xenoliths via the following chemical reactions: $2SiO_2 + CaMg(CO_3)_2 \rightarrow CaMg(SiO_3)_2 + 2CO_2$, $4SO_2+4H_2O \rightarrow 3H_2SO_4+H_2S$ (Figure 1B). Assemblages of sulfate inclusions, silicate melt inclusions, calc-silicate inclusions, and CO_2-vapor inclusions and the sulfate melt inclusions hosted in diopside record these reactions. Finally, as the temperature decreases, the widespread calc-silicate minerals crystalize into inclusions in quartz and anhydrite or constitute sporadic endoskarns at Chating. Ca-rich sulfate melts occur as sulfate melt inclusions via removing excess CaO, and form abundant anhydrite due to the addition of brines (Figure 1C).

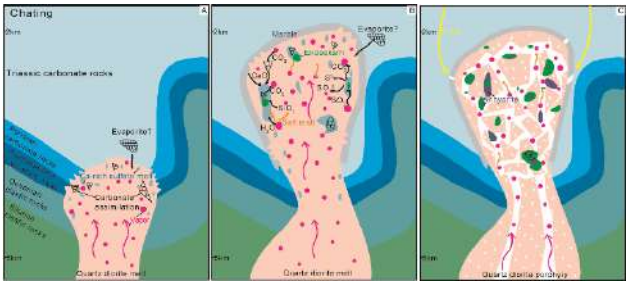

Figure 1. Schematic cross-section showing endoskarn formation at Chating. A: Silicate melts is intruding into carbonate strata, inducing carbonate assimilation and Ca-rich sulfate melts. B: Silicate melts emplaced into carbonate strata, inducing marble formation and contact metasomatism. C: Silicate melts crystalized, endoskarns occurred, and breccia is formulating.

REFERENCES

Carter, L., Dasgupta, R. (2016) Effect of melt composition on crustal carbonate assimilation: Implications for the transition from calcite consumption to skarnification and associated CO2 degassing, Geochemistry, Geophysics, Geosystems, 17.

Gaeta, M. et al. (2009) Carbonate assimilation in open magmatic systems: the role of melt-bearing skarns and cumulate-forming processes, J. of Petrology 50, 361–385.

Lentz, D. R. (1999) Carbonatite genesis: a reexamination of the role of intrusion-related pneumatolytic skarn processes in limestone melting, Geology 27, 335–338.
Lentz, D. R. (2005) Mass-balance analysis of mineralized skarn systems: Implications for replacement processes, carbonate mobility, and permeability evolution.
Whitley, S. et al. (2020) Magmatic and Metasomatic Effects of Magma–Carbonate Interaction Recorded in Calc-silicate Xenoliths from Merapi Volcano (Indonesia), J. of Petrology 61.

High-temperature inclusions in IOA and IOCG-type deposits

Xinyue Xu[1,2], Matthew Steele-MacInnis[1], Wyatt Bain[3], Marko Szmihelsky[1]

[1] *Department of Earth and Atmospheric Sciences, University of Alberta, 1-26 Earth Sciences Building, Edmonton, T6G2E3, Canada*

[2] *School of Resources and Environmental Engineering, Hefei University of Technology, 193 Tunxi Road, Hefei, 230009, China*

[3] *Department of Geology, Lakehead University, Thunder Bay, ON P7B 5E1, Canada*

E-mail: xxu20@ualberta.ca

Iron oxide-apatite (IOA) and iron oxide-copper-gold (IOCG) deposits are an important group of economic iron oxide-rich deposits in the world. IOA and IOCG-type deposits are often associated, and the characterization and origin of mineralizing fluids are still poorly understood. To address these debates, we analyzed high-temperature fluids and melt inclusions in numerous samples of iron oxide-related deposits from the USA, Argentina, Chile, China, and Iran.

We report several types of inclusions hosted in apatite, anhydrite, diopside, and quartz, such as hypersaline inclusions, calc-silicate inclusions, sulfate melt inclusions, carbonate melt inclusions, and silicate inclusions (Figure 1). Most of these inclusions contain various crystalline phases and solids, chlorides (sylvite, halite, hibbingite, etc), sulfates (anhydrite, cesanite, and barite), oxide (hematite and magnetite), and silicate (feldspars, quartz, wollastonite, diopside, actinolite, etc) are identified based on laser Raman analysis and energy dispersive spectroscopy (EDS). The homogenization temperatures of these inclusions are generally between 650° and 1250° C. Hence, several populations in the IOA-IOCG system were defined in this study: hypersaline fluids, carbonate-sulfate melts, calc-silicate melts, and silicate melts.

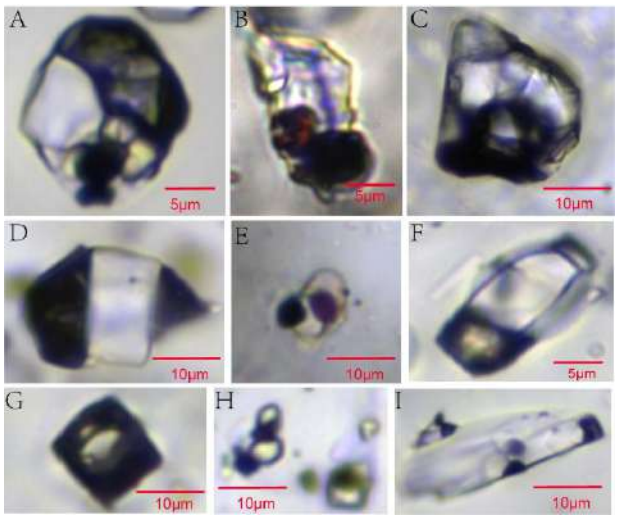

Figure 1. Photographs of different types of inclusions. A, B: Hypersaline inclusions; C, D: Sulfate melt inclusions; E: Carbonate melt inclusions; F, G: Silicate melt inclusions; H, I: Calc-silicate melt inclusions.

Bain et al. (2020; 2021) emphasized the critical role played by carbonate-sulfate melts in the formation of magnetite-apatite deposits, however, these different types of inclusions were largely ignored by most authors. The different systems of fluids and melts represented by these inclusions may play an important role in transporting metals, and to some extent reflect the interaction of magma with other environments such as carbonates and evaporites. Overall, the key implication of this study is that attention should be paid to the study of high-temperature inclusions in these deposits in order to clarify their key role in mineralization and bring a breakthrough in the study of the genesis mode of IOA and IOCG-type deposits.

REFERENCES

Bain, W.M. et al. (2020) A fundamental role of carbonate-sulfate melts in formation of iron oxide-apatite deposits, Nat. Geosci. 13, 751-757.

Bain, W.M. et al. (2021) Evidence for iron-rich sulfate melt during magnetite-(apatite) mineralization at El Laco, Chile, Geology 49, 1044-1048.